Title

Energy-Based Liquefaction Evaluation: The Port of Kushiro in Hokkaido, Japan, 2003 Tokachi-Oki Earthquake

Journal

Journal of Geotechnical and Geoenvironmental Engineering, 150(10)

ISSN

1090-0241 1943-5606

Authors

Ko, Kil-Wan
Kayen, Robert E
Kokusho, Takaji
et al.

Publication Date

2024-10-01

DOI

10.1061/JGGEFK.GTENG-11989

Peer reviewed

Case Study

Energy-Based Liquefaction Evaluation: The Port of Kushiro in Hokkaido, Japan, 2003 Tokachi-Oki Earthquake

Kil-Wan Ko[1]; Robert E. Kayen, M.ASCE[2]; Takaji Kokusho[3]; Makbule Ilgac, M.ASCE[4]; Atsushi Nozu[5]; and Chukwuebuka C. Nweke, M.ASCE[6]

Abstract: The magnitude (M_w) 8.3 Tokachi-oki earthquake occurred in September 2003, causing extensive damage in Hokkaido, Japan, and triggering extensive soil liquefaction in the region. The Port of Kushiro was one of the locations where surficial evidence of liquefaction was observed but was also a well-instrumented location with four pore-water pressure transducers installed in the backfill of the quay wall. However, all of the sensors malfunctioned during the earthquake. As a result, the pore-water pressure response recorded by those sensors were inaccurate and unusable with regard to evaluating liquefaction triggering and extent. This study introduced the energy-based soil liquefaction evaluation to estimate the excess pore water pressure responses at the Port of Kushiro based on the cumulative strain energy of the soil during the 2003 Tokachi-oki earthquake. In order to apply the energy-based method to this case history, this study explored the empirical equation describing a relationship between normalized cumulative energy and excess pore water pressure ratio while incorporating the bidirectional shaking effect on strain energy development. Although the energy-based method allowed for the estimation of the time needed to trigger liquefaction at a target site, it was derived using the empirical coefficients that were developed for a different soil from those at the site of interest. This indicated that an adjustment to the estimated timing of liquefaction was needed, which was accomplished by additional evaluation through a Stockwell transform and Arias intensity-based liquefaction assessment. Both procedures indicated a similar timing of liquefaction at the site. Based on the updated time of liquefaction triggering, the empirical coefficient was recalibrated to estimate the excess pore water pressure ratio, and the result provided reasonable excess pore water pressure responses at the backfill of the Port of Kushiro during the 2003 Tokachi-oki earthquake. **DOI: 10.1061/JGGEFK.GTENG-11989.** *© 2024 American Society of Civil Engineers.*

Author keywords: Soil liquefaction; 2003 Tokachi-oki earthquake; Case history; Excess pore water pressure ratio; Energy-based liquefaction evaluation.

Introduction

The Tokachi-oki earthquake in 2003 was a moment magnitude (M_w) 8.3 event that occurred on September 26, 2003, off the coast of Hokkaido, Japan (Sasajima et al. 2005). The earthquake impacted the entire area of Hokkaido and caused extensive damage. In particular, earthquake-induced soil liquefaction rendered subsequent damage to the structures nearby and at distances reaching about 200 km from the epicenter (Koyamada et al. 2006). For example, soil liquefaction resulted in large-scale failure of embankments filled with soils containing volcanic ash in the Kyowa area of Tanno Town, situated about 230 km away from the epicenter (Yamashita et al. 2005). During the earthquake, liquefaction was widespread at the Port of Kushiro, located in Eastern Hokkaido, Japan. Surface evidence of liquefaction triggering, such as sand boils and ground fissures, was observed in the backfill of the Port site, where numerous accelerometers and pore pressure transducers were installed.

The 2003 Tokachi-oki earthquake, similar to other earthquake case histories, further highlighted the severity of liquefaction-induced damage to infrastructure (Bartlett and Youd 1995; Ishihara and Koga 1981; Kim et al. 2021; Yamaguchi et al. 2012). In engineering practice, liquefaction assessment consists of three steps: characterizing the susceptibility of the subsurface materials, estimating the "triggering" given the seismic demands, and evaluating the consequences. With regard to triggering at a site, the stress-based method assesses the liquefaction potential of the soil based on a relation between the applied cyclic stress ratio (CSR) and cyclic stress capacity of the soil, which is cyclic resistance ratio (CRR) (Boulanger and Idriss 2014; Cetin et al. 2018a; Youd and Idriss 2001). In most seismic design codes, the factor of safety, which is a ratio of CRR to CSR, is commonly used to evaluate the liquefaction potential of the site (CEN 2004; FEMA 2009; Zhang et al. 2021). Recently, many researchers have developed probabilistic assessment tools for evaluating soil liquefaction by taking into account the uncertainties of CSR and site information (Moss et al. 2006; Kayen et al. 2013; Boulanger and Idriss 2014; Cetin et al. 2018a). Because CRR is a function of the number of

[1]Postdoctoral Researcher, Dept. of Civil and Environmental Engineering, Univ. of Southern California, Los Angeles, CA 90089-2531 (corresponding author). ORCID: https://orcid.org/0000-0001-5916-4227. Email: kilwanko@usc.edu

[2]Professor, Dept. of Civil and Environmental Engineering, Univ. of California, Berkeley, Berkeley, CA 94720. ORCID: https://orcid.org/0000-0002-0356-072X. Email: rkayen@berkeley.edu

[3]Emeritus Professor, Dept. of Civil and Environmental Engineering, Chuo Univ., 46-5-1504 Senju-Asahicho, Adachi-ku, Tokyo 120-0026, Japan. Email: koktak@ad.email.ne.jp

[4]Postdoctoral Researcher, Dept. of Civil and Environmental Engineering, Univ. of California, Berkeley, Berkeley, CA 94720. ORCID: https://orcid.org/0000-0002-3459-2361. Email: makbuleilgac@berkeley.edu

[5]Director, Dept. of Earthquake Disaster Prevention Engineering, Port and Airport Research Institute, 3-1-1 Nagase, Yokosuka 239-0826, Japan. Email: nozu@p.mpat.go.jp

[6]Assistant Professor, Dept. of Civil and Environmental Engineering, Univ. of Southern California, Los Angeles, CA 90089-2531. Email: chukwueb@usc.edu

Note. This manuscript was submitted on June 2, 2023; approved on April 23, 2024; published online on July 23, 2024. Discussion period open until December 23, 2024; separate discussions must be submitted for individual papers. This paper is part of the ***Journal of Geotechnical and Geoenvironmental Engineering***, © ASCE, ISSN 1090-0241.

loading cycles and effective overburden stress, the simplified stress-based method requires a overburden stress correction factor and a magnitude scaling factor accounting for the number of equivalent stress cycles (Cetin and Bilge 2012).

The energy-based method for evaluating liquefaction potential has been studied since Nemat-Nasser and Shokooh (1979) and Davis and Berrill (1982), resulting in the development of a correlation between pore-water pressure increase and strain energy dissipated by the soil. An underlying principle of the method is that liquefaction is triggered when the work dissipated by the soil exceeds the energy capacity of the soil needed to resist liquefaction (Nemat-Nasser and Shokooh 1979). The performance of the energy-based method in determining liquefaction potential has been evaluated by multiple investigators through laboratory experiments such as cyclic torsional shear tests (Jafarian et al. 2012; Towhata and Ishihara 1985) and cyclic triaxial tests (Kokusho 2013; Kokusho and Tanimoto 2021). The cumulative dissipated energy normalized by the effective stress of the soil has a unique correlation with liquefaction-relevant parameters, such as the excess pore water pressure ratio r_u (i.e., a ratio of excess pore water pressure Δu to the initial effective stress of the soil σ') (Polito et al. 2013, 2008; Towhata and Ishihara 1985), and the liquefaction-induced strain and surface settlement (Kokusho 2021). It implies that the energy-based method adequately captures the fundamental behavior of liquefiable soils by combining the effect of the number of cycles and applied stress. Given that the energy-based method is applicable to both harmonic and irregular loadings (Kokusho and Kaneko 2018), it is conveniently compatible with case history evaluation due to the irregularity of seismic waves with regard to amplitude and frequency.

Regarding field application, liquefaction evaluation should consider the effect of bidirectional earthquake motions because the liquefaction potential significantly changes when two horizontal motions are considered simultaneously (Ghaboussi and Dikmen 1981). Seed et al. (1978) suggested using 80%–90% of the cyclic shear stresses needed to initiate liquefaction as an appropriate single component that expresses the effect of bidirectional shaking. Using a biaxial shaking table for centrifuge tests, Su and Li (2008) claimed that the peak excess pore water pressures under bidirectional shaking were 0%–20% greater than those under unidirectional shaking, which supports the result by Seed et al. (1978). Jin and Guo (2021) discussed the effect of the phase difference between two horizontal motions on the liquefaction and stated that the liquefaction resistance under bidirectional shaking decreased to 70% of that under unidirectional shaking. However, El Shafee et al. (2017) proved that increasing the uniaxial shaking by 10% underestimated the real response of the soil under bidirectional shaking impacts, which imposed more energy demand on the soil. Instead of using a reduction factor for a single equivalent component, the use of an energy-related parameter as a scalar quantity facilitates the combination of two horizontal motions (Kayen and Mitchell 1997), whereas using cyclic shear stresses for the stress-based method should intrinsically consider the directivity of the shaking as a vector quantity when synthesizing the effect of two horizontal motions. Hence, the energy-based method is particularly suitable for assessing soil liquefaction in case histories where recorded ground motions have two horizontal components because the method accurately reflects the soil's real response to bidirectional shaking.

The objective of this study is to present a unique case history at the Port of Kushiro assessing pore pressure characteristics during the 2003 Tokachi-oki earthquake and propose an energy-based liquefaction evaluation at this site. This study explored the use of the energy-based method to estimate the pore water pressure in the backfill of the quay wall at the Port of Kushiro in Hokkaido during the 2003 Tokachi-oki earthquake. First, the stress-based method was used to identify liquefiable layers in the backfill during the earthquake. Next, to estimate r_u from the calculated strain energy, an empirical equation describing a relationship between cumulative strain energy dissipated by soil and r_u was developed from the previous literature using torsional shear tests. The cumulative energies differed depending on which methodology was used to assess bidirectional shaking: root sum squared (RSS), maximum rotated acceleration (RotD100), and geometric mean. Then, the calculated strain energy was converted into r_u over time through the empirical curves. At the same time, Stockwell transforms (i.e., the time-frequency response) of the horizontal motions were employed to estimate the timing of liquefaction. Moreover, the Arias intensity-based liquefaction evaluation curves (Kayen and Mitchell 1997) served as a reference that helped to certify the accurate timing of soil liquefaction. Finally, the timing of liquefaction was used to tune the estimation of r_u by recalibrating the coefficient of the empirical curves.

Port of Kushiro and Tokachi-Oki Earthquake in 2003 (M_W, 8.3)

Port of Kushiro

The Port of Kushiro is located in Eastern Hokkaido, Japan [Fig. 1(a)]. In the decade prior to the 2003 Tokachi-oki earthquake, the Port of Kushiro was struck by three major earthquakes, (1993 Kushiro-oki, $M_w = 7.6$; 1993 Hokkaido Nansei-oki, $M_w = 7.7$; and 1994 Hokkaido Toho-oki, $M_w = 8.3$). The 1993 Kushiro-oki and 1994 Hokkaido Toho-oki earthquakes caused damage to the quay walls because the backfill soil liquefied. Considering the high susceptibility of the backfilled soil to liquefaction and the increased likelihood of more potential damage to the quay walls, a project test site was constructed by Hokkaido Regional Development Bureau, Ministry of Land, Infrastructure, Transport and Tourism, Japan, along the quay walls at Pier No. 4 at the Port of Kushiro. The project deployed many sensors (i.e., accelerometers, velocimeters, porewater pressure transducers, etc.) in the backfill [Fig. 1(b)] to investigate the effect of soil liquefaction on the dynamic behavior of the quay wall.

The project consisted of two quay walls, with one corresponding to untreated backfill and the other to treated backfill against liquefaction. They were separated by a horizontal distance of 11.5 m in the east-west direction [Fig. 1(b)]. The untreated and treated sections of the test quay walls included deeper sand layers (As1 and As2) overlain by the quay wall with adjacent rubble backing and backfill sand [Fig. 1(c)]. An accelerometer was placed in each of the deeper sand layers, and multiple accelerometers and pore-water pressure transducers were installed within the backfill. The backfill of the treated quay wall underwent ground improvement via sand compaction piles to enhance its liquefaction resistance between the depths of 2.44 and 11.14 m. This study used sensors located in three vertical arrays: two arrays in the untreated backfill and one array in the treated backfill. Four accelerometers were employed, including TA8 (located in the As2 sand layer at a depth of 16.9 m), TA7 (located in the As1 sand layer at a depth of 11.9 m), UA6 (located in the backfill sand collocated with the pore-water pressure transducer UP2 at a depth of 5.44 m), and UA5 at the backfill ground surface. TA7, TA8, and UA5 were positioned in the same location in the north–south direction [Fig. 1(b)]. The sand layers, As1 and As2, where TA7 and TA8 were installed, respectively, were not treated against liquefaction. Sasajima et al. (2005) described the details of the project related to the Port of Kushiro and the test quay walls.

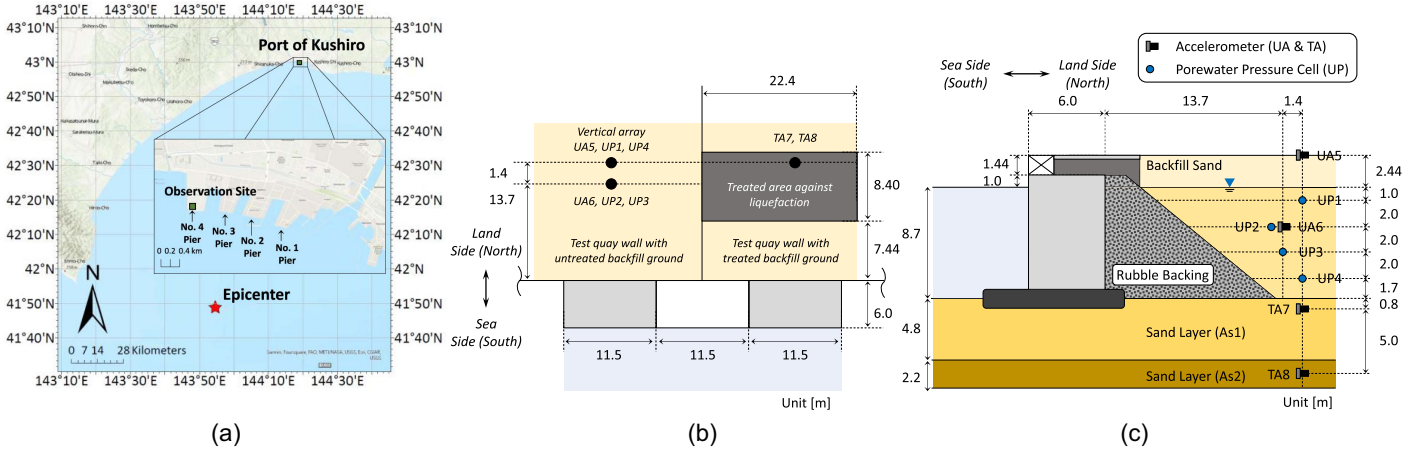

(a) (b) (c)

Fig. 1. Target site at the Port of Kushiro: (a) epicenter of the 2003 Tokachi-oki earthquake and observation site at the Port of Kushiro (map from Garmin, Foursquare, FAO, METI/NASA, USGS, ESRI, CGIAR, USGS); (b) top view of the Kushiro port site; and (c) cross-section of the quay wall and instrumentation at the site.

The Performance of the Port of Kushiro during 2003 Tokachi-Oki Earthquake

The 2003 Tokachi-oki earthquake occurred 140 km to the south-southwest from the Port of Kushiro [Fig. 1(a)]. In the Port of Kushiro, Hokkaido, ground fissures and sand boils were observed on the ground surface of the quay wall backfill (Sasajima et al. 2004). The quay wall and backfill experienced a permanent horizontal displacement of 15 cm toward the seaside during the earthquake. The strong shaking duration $D_{5\text{-}95}$ (the time difference between the 5% and 95% Arias intensity I_a) was 52.5 s based on the acceleration records from TA8 (i.e., 5% of I_a started at 44 s, and 95% of I_a is at 96.5 s). The average peak ground accelerations (PGAs) of two horizontal motions in the sand were 0.174 and 0.176 g, corresponding to UA5 and UA6 records, respectively [Figs. 2(a–d)]. The measured acceleration responses depicted period elongation (i.e., the frequency reduction due to soil softening by liquefaction) to initiate around 50 s (Kramer et al. 2016). Time–frequency responses using Stockwell transforms, which reveal the timing of liquefaction of the backfill soil, will be discussed in detail in the section "Time-Frequency Response of Liquefied Soil Layer." The measured pore water pressure in the backfill, however, was substantially lower than the level of the initial effective stress, such that the r_u responses for UP1–UP4 were lower than 1 [Figs. 2(e–h)]. The maximum value of r_u was lower than 0.5, and the pore water pressure development kept increasing even after 96.5 s, corresponding to 95% of I_a, which implied almost the end of the shaking. As Sasajima et al. (2005) reported, the measured pore water pressure transducers failed to record the pore-water pressure rise during the earthquake shaking due to a malfunction in the filtering of all the fluid pressure sensors. Accordingly, this study aimed to estimate the pore water pressure responses based on the strain energy dissipated by the soil.

Stress-Based Soil Liquefaction Evaluation

Prior to applying the energy-based method to the site, the stress-based method was used to evaluate the liquefaction potential and pore water pressure buildup of the backfill as a pre-evaluation first estimate. The standard penetration test (SPT)–based soil liquefaction evaluation (Cetin et al. 2018b) was used. To convert the SPT N-profile to the SPT $(N_1)_{60}$ value, this study adopted an energy ratio of 78%, as proposed by Seed et al. (1985). The SPT $(N_1)_{60}$ value in the backfill below the water table was less than 8, implying a high potential for soil liquefaction during major earthquake events (Sasajima et al. 2005). The SPT $(N_1)_{60}$ value sharply decreased from approximately $(N_1)_{60} = 13$ immediately above the water table at 2.44 m to $(N_1)_{60} = 6$ on average [Fig. 3(a)]. In order to estimate the relative density (D_r) of the backfill, the empirical relationship between $(N_1)_{60}$ and D_r was used (Idriss and Boulanger 2010)

$$D_r = \sqrt{\frac{(N_1)_{60}}{46}} \tag{1}$$

The estimated D_r of the backfill is illustrated in Fig. 3(b).

The triggering evaluation curve, based on the SPT N-value from Cetin et al. (2018b), was used to provide an approximation of CRR for the backfill [Fig. 3(c)]. In order to obtain the CSR profile during the 2003 Tokachi-oki earthquake, we followed two alternative approaches, as described by Cetin et al. (2018a, b): equivalent linear site response analyses and the simplified approach [using stress reduction factors by Cetin and Seed (2004)]. Nonlinear effective site response analyses of a one-dimensional soil column were also conducted only to evaluate pore water pressure responses and acceleration time histories at the site using DEEPSOIL (Hashash et al. 2020). The unit weights of the soil for each layer were estimated from the SPT-N value (Cetin et al. 2018a). Shear wave velocities (V_s) for each layer were determined through the SPT–N and V_s correlation for sand, as described by Cetin et al. (2018b)

$$V_s = 80 \times N^{1/3} \tag{2}$$

This correlation is specific to sand, and the resulting V_s units are in m/s. For the nonlinear effective stress analysis, this study employed the GQ/H model (Groholski et al. 2016), Vucetic and Dobry (1986) pore pressure generation model. The input information and parameters were computed based on empirical relationships outlined in the DEEPSOIL user manual (Hashash et al. 2020). The model parameters for the site response analyses are summarized in Table 1. In this analysis, the mean and lower limit curves from Seed and Idriss (1970) were adopted as normalized modulus reduction and damping curves for soil layers [Fig. 4(a)]. The lower curves were applied to layers with vertical effective stress less than 1 atm, whereas the mean curves were used for layers with vertical effective stress greater than 1 but smaller than 3 atm. The simplified method used peak ground accelerations of surface motion records

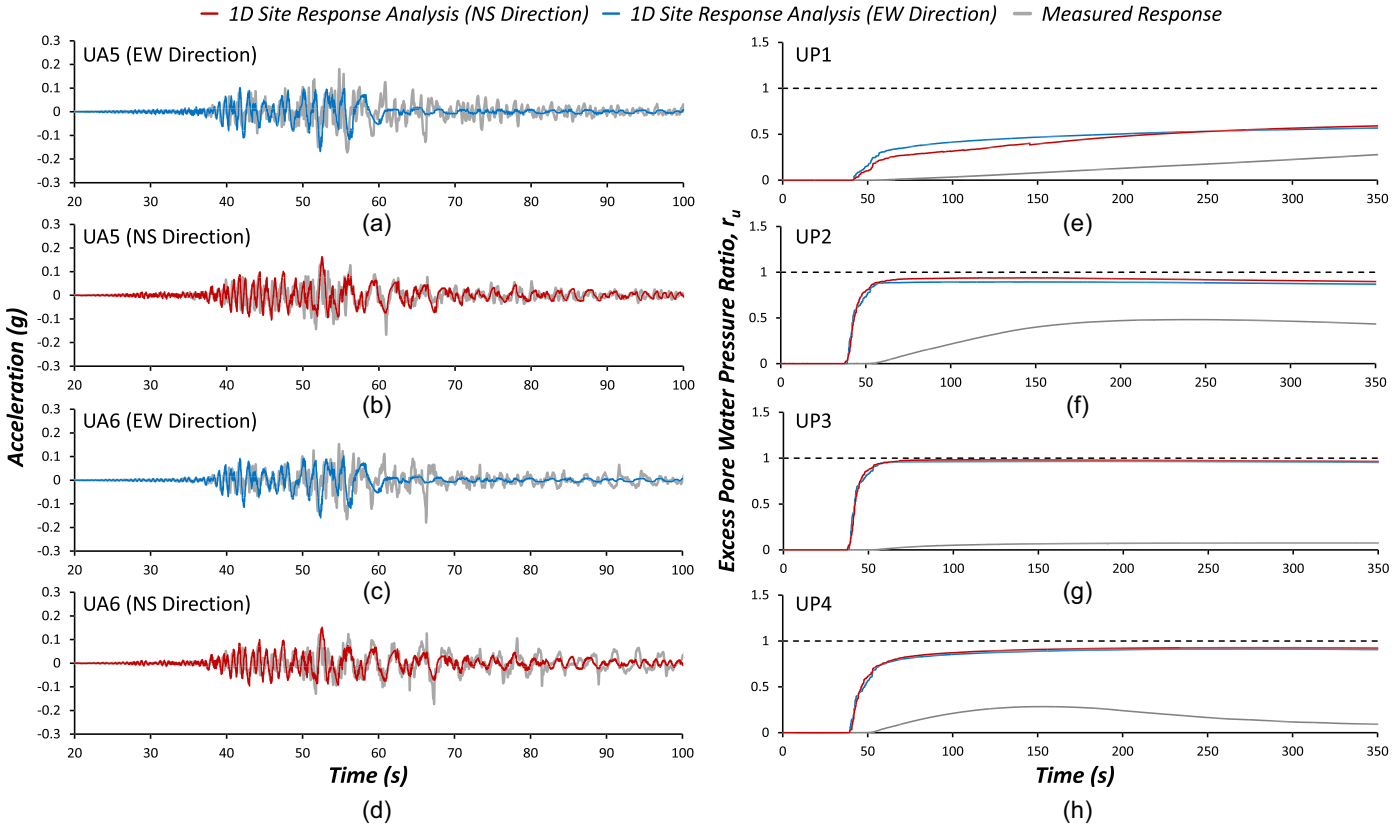

Fig. 2. Seismic responses of backfill sand of the quay wall during the 2003 Tokachi-oki earthquake: (a–d) measured acceleration records and estimated acceleration responses from one-dimensional nonlinear site response analyses in two horizontal motions at the soil surface and the depth of 5.44 m; and (e–h) measured excess pore water pressure ratio (r_u) of UP1 to UP4 and estimated responses from one-dimensional nonlinear site response analyses in two horizontal motions: (a) UA5 (EW Direction); (b) UA5 (NS Direction); (c) UA6 (EW Direction); (d) UA6 (NS Direction); (e) UP1; (f) UP2; (g) UP3; and (h) UP4.

obtained from UA5. The site response analyses used acceleration records from TA8 in the As2 layer as an input within motion [Figs. 4(b and c)]. TA8 recorded the deepest acceleration response at this site, and the stress-based liquefaction evaluation indicated that the As2 layer did not liquefy during the earthquake.

The nonlinear effective site response analysis results were similar to the measured response [Figs. 2(a–d)]. The differences in PGA between measured and estimated responses for UA5 were less than 7%, whereas for UA6, they were less than 13% (Table 2). However, the differences in I_a were significantly larger than those in PGA. The CSR was estimated as the geometric mean of CSRs obtained from the equivalent linear site response analyses and the simplified method in the E–W and N–S directions [Fig. 3(c)]. The stress-based method resulted in a factor of safety profile (i.e., CRR/CSR) estimating the possibility of liquefaction triggering from the depth of the water table at 3.24 m to a depth of approximately 12.67 m [Fig. 3(d)]. The probability of liquefaction by Cetin et al. (2018b) indicated 100% liquefaction occurrence between the depths of 3.74 and 11.7 m for both equivalent linear site response analyses and the simplified method. Accordingly, estimated r_u responses from the nonlinear effective stress analysis exhibited triggering of liquefaction in the backfill of the Kushiro port spanning UP2 to UP4 responses [Figs. 2(e–h)]. The surficial manifestation at the site, including ground fissures and sand boils, already indicated problematic pore water pressure responses. This pre-evaluation analysis, conducted using the stress-based procedure, supplements the field observations and demonstrates that the simplified approach appropriately indicates the susceptibility of the loose sand to excessive pore pressure buildup due to the imposed cyclic loading.

Energy-Based Method for Liquefaction Evaluation

Earthquakes cause undrained cyclic behavior of liquefiable soil, and the area of the hysteresis attributed to cyclic behaviors implies the strain energy dissipated by the soil. Using the relationship between r_u and the normalized cumulative strain energy from shear stress–strain loops, the accumulation of the strain energy over time in the soil layer was used to determine the r_u of the soil layer during the earthquake (Ko and Kayen 2024). Using acceleration time histories, measured by vertically aligned accelerometers, the shear stress (τ) and strain (γ) responses of the soil can be estimated. Hence, the recorded acceleration responses during earthquakes provide the cumulative strain energy over time, derived from the estimated stress–strain hysteresis loop. This, in turn, further leads to r_u time-histories of the soil layer through the empirical relationship between the cumulative strain energy and r_u. Unlike most laboratory tests, there are two components of horizontal loading (bidirectional irregular horizontal loading sources) being applied to the soil at the site during an earthquake. This section will discuss a step-by-step procedure to estimate r_u time history from the acceleration records and a method to treat bidirectional shaking from case histories for the energy-based liquefaction method.

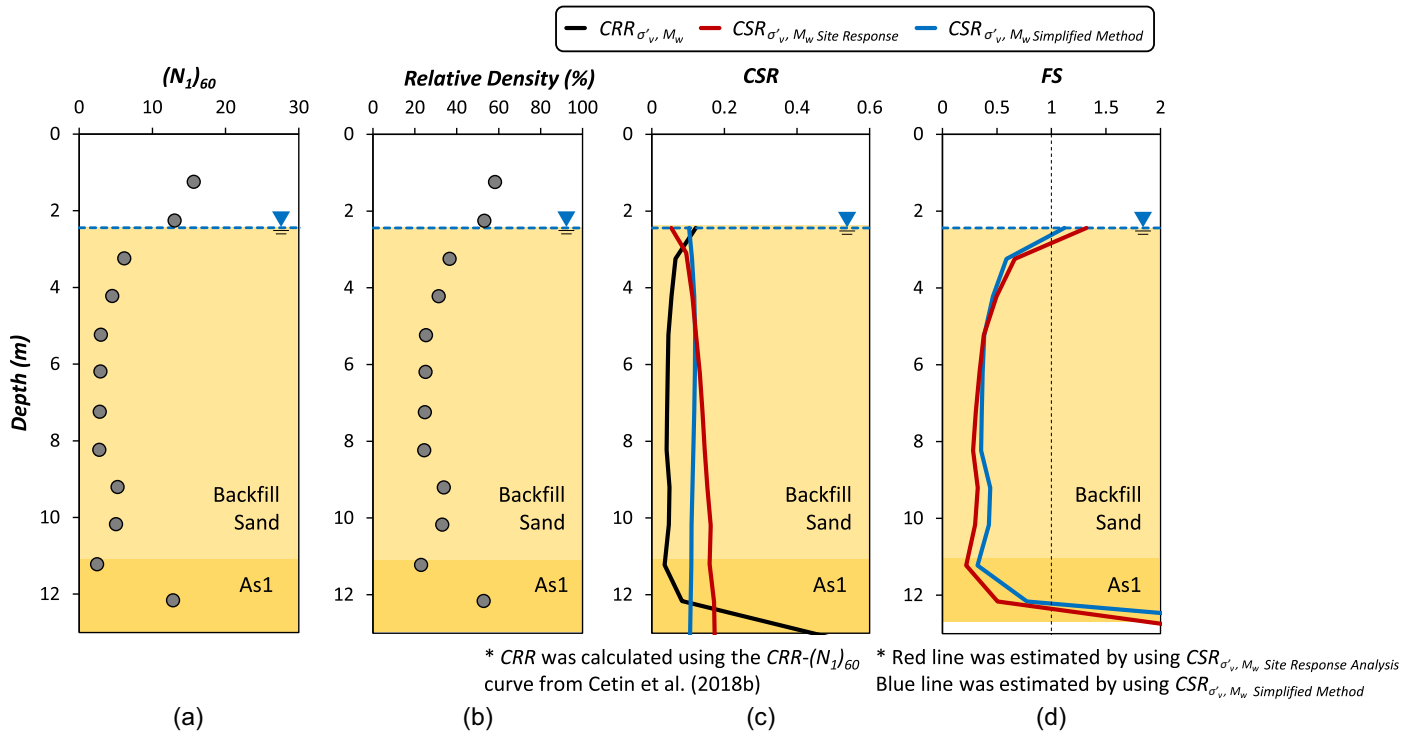

Fig. 3. Stress-based liquefaction evaluation for the backfill of the quay wall: (a) SPT $(N_1)_{60}$ profile; (b) estimated relative density; (c) cyclic stress ratio from equivalent linear site response analyses and the simplified method and cyclic resistance ratio at the backfill during the 2003 Tokachi-oki earthquake; and (d) factor of safety profile at the site.

Table 1. Parameters for site response analyses

Depth (m)	Thickness (m)	Unit weight (kN/m^3)	SPT $-(N_1)_{60}$	Vertical effective stress (kPa)	Shear wave velocity (m/s)	Parameters for Vucetic and Dobry (1986) model						
						Max. r_u	C_v (m^2/s)	f	F	s	p	γ (%)
0.00–1.25	1.25	18.9	16	11.81	160.00	0.99	0.00929	1	1.46	1.01	1	0.02
1.25–2.44	1.19	18.9	13	34.87	160.00	0.99	0.00929	1	1.46	1.01	1	0.02
2.44–3.74	1.30	18.9	6	52.02	126.99	0.99	0.00929	1	2.09	1.01	1	0.02
3.74–4.73	0.99	17.3	5	61.64	115.38	0.99	0.00929	1	2.42	1.01	1	0.02
4.73–5.72	0.99	17.3	3	69.06	100.79	0.99	0.00929	1	2.99	1.01	1	0.02
5.72–6.72	1.00	17.3	3	76.51	100.79	0.99	0.00929	1	2.99	1.01	1	0.02
6.72–7.73	1.01	17.3	3	84.04	100.79	0.99	0.00929	1	2.99	1.01	1	0.02
7.73–8.72	0.99	17.3	3	91.53	100.79	0.99	0.00929	1	2.99	1.01	1	0.02
8.72–9.69	0.97	18.9	5	99.64	126.99	0.99	0.00929	1	2.09	1.01	1	0.02
9.69–10.70	1.01	18.9	5	108.64	126.99	0.99	0.00929	1	2.09	1.01	1	0.02
10.70–11.70	1.00	17.3	2	116.98	100.79	0.99	0.00929	1	2.99	1.01	1	0.02
11.70–12.67	0.97	20.5	13	125.91	177.92	0.99	0.00929	1	1.24	1.01	1	0.02
12.67–13.62	0.95	21.5	35	136.64	251.31	0.99	0.00929	1	0.73	1.01	1	0.02
13.62–14.55	0.93	21.5	26	147.63	230.76	0.99	0.00929	1	0.83	1.01	1	0.02
14.55–15.54	0.99	21.5	28	158.85	240.00	0.99	0.00929	1	0.78	1.01	1	0.02
15.54–16.52	0.98	21.5	60	170.37	313.19	0.99	0.00929	1	0.52	1.01	1	0.02
16.52–16.94	0.42	21.5	59	178.55	313.19	0.99	0.00929	1	0.52	1.01	1	0.02

Note: C_v = coefficient of consolidation; f = dimensionality parameter; $F = 3{,}810 \times V_s^{-1.55}$, curve fitting parameter; $s = (\text{Fines content} + 1)^{0.1252}$, curve fitting parameter; p = curve fitting parameter; and γ = threshold shear strain.

Step-by-Step Procedure of Energy-Based Method to Estimate r_u at a Site

The energy-based method requires knowledge of the soil density (ρ), vertically aligned acceleration records in order to obtain the $\tau - \gamma$ cyclic responses, and an empirical relationship between r_u and the normalized cumulative strain energy. The step-by-step procedure of the energy-based method is as follows:

1. Obtain the two horizontal acceleration time histories $\ddot{u}_i(t)$ and $\ddot{u}_{i-1}(t)$] from the vertically aligned accelerometers in the liquefiable soil layer. The installed depth of the ith and $(i-1)$th accelerometers are h_i and h_{i-1}. The distance between the vertically aligned accelerometers measuring $\ddot{u}_i(t)$ and $\ddot{u}_{i-1}(t)$ is $\Delta h_{i-1} = h_i - h_{i-1}$.
2. Compute the time-varying $\tau_{i-1/2}(t)$ and $\gamma_{i-1/2}(t)$ of the soil layer at level $(h_i + h_{i-1})/2$ (Zeghal et al. 2018). The value of $\gamma_{i-1/2}(t)$ is calculated as follows:

$$\gamma_{i-1/2}(t) = \frac{u_i(t) - u_{i-1}(t)}{\Delta h_{i-1}}, \quad i = 2, 3, \ldots \tag{3}$$

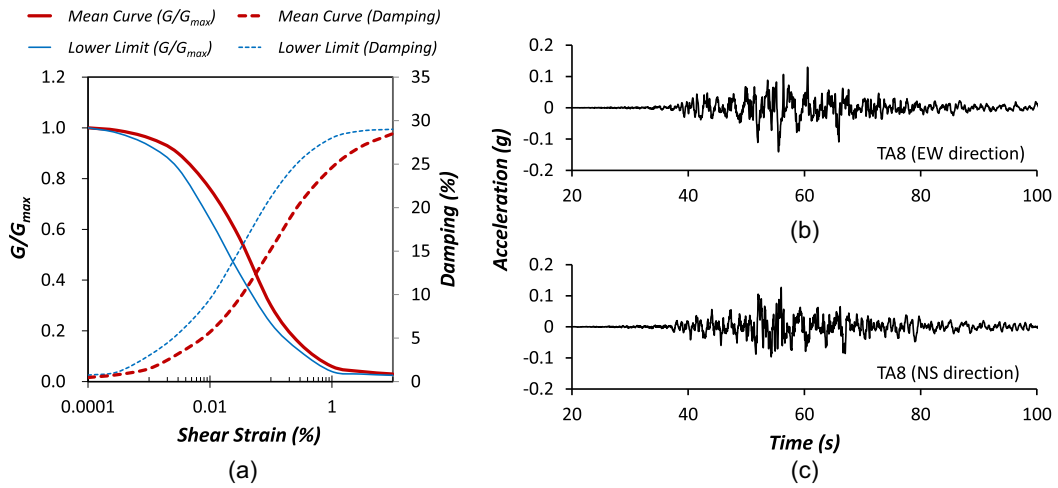

Fig. 4. Shear modulus reduction curves, damping curves, and input motions for nonlinear effective site responses analysis: (a) modulus reduction and damping curves obtained from Seed and Idriss's (1970) mean and lower limit curves; (b) acceleration time history of TA8 EW direction; and (c) acceleration time history of TA8 NS direction.

Table 2. Comparison between measured and estimated acceleration responses from the nonlinear site response analysis

		Peak ground acceleration, PGA (g)			Arias intensity, I_a (m/s)		
Accelerometer	Depth (m)	Measured response	Site response analysis	Difference (%) (site response analysis/ measured response)	Measured response	Site response analysis	Difference (%) (site response analysis/ measured response)
UA5 (N–S)	0, surface	0.167	0.163	2.4	1.053	1.215	15.4
UA5 (E–W)	0, surface	0.180	0.168	6.9	1.500	0.973	35.1
UA6 (N–S)	5.44	0.173	0.152	12.3	1.883	1.118	59.4
UA6 (E–W)	5.44	0.179	0.159	11.6	1.369	0.898	34.4

where $u_i(t)$ and $u_{i-1}(t)$ = double-integrated displacement time histories from the acceleration records. The shear stress (τ_i) at level h_i of the ith accelerometer is calculated as follows:

$$\tau_i(t) = \tau_{i-1}(t) + \rho \frac{\ddot{u}_{i-1} + \ddot{u}_i}{2} \Delta h_{i-1}, \quad i = 2, 3, \ldots \tag{4}$$

where τ at the soil surface $= 0$. Shear stress ($\tau_{i-1/2}$) at the midpoint between ith and $(i-1)$th accelerometers, indicating the representative shear stress of the layer, is estimated through linear interpolation as

$$\tau_{i-1/2}(t) = \tau_{i-1}(t) + \rho \frac{3\ddot{u}_{i-1} + \ddot{u}_i}{8} \Delta h_{i-1}, \quad i = 2, 3, \ldots \tag{5}$$

For the energy-based method, $\tau_{i-1/2}(t)$ and $\gamma_{i-1/2}(t)$ are used to obtain the hysteresis loops.

3. Calculate the change in dissipated energy ΔW over time and the cumulative dissipated energy ($\Sigma\Delta W$) change normalized by effective stress (σ'_{vc}) of the soil layer ($\Sigma\Delta W/\sigma'_{vc}$). The trapezoidal rule calculates $\Sigma\Delta W$ as follows (Millen et al. 2021):

$$\tau_{avg,j} = \begin{cases} \dfrac{|\tau_{j+1} + \tau_j|}{2}, & \tau_{j+1} \cdot \tau_j \geq 0 \\ \dfrac{\tau_{j+1}^2 + \tau_j^2}{2 \cdot |\tau_{j+1} - \tau_j|}, & \tau_{j+1} \cdot \tau_j < 0 \end{cases} \tag{6}$$

$$\Sigma\Delta W = \sum_{j=1}^{n-1} \tau_{avg,j}(\gamma_{j+1} - \gamma_j) \tag{7}$$

where τ_j and τ_{j+1} = shear stress at each time step of jth and $j+1$th, respectively; γ_j and γ_{j+1} = shear strain at each time step of jth and $j+1$th, respectively; and $\Sigma\Delta W$ = cumulative strain energy dissipated by soil per unit volume, and its unit is N/m^2. Applied and recovered strain energy during the soil's cyclic behavior are automatically inclusive to Eq. (6) due to the sign changes of τ and γ during earthquakes (Fig. 5) (Millen et al. 2021).

4. Estimate r_u using an empirical equation for the $\Sigma\Delta W/\sigma'_{vc} - r_u$. The following section will discuss the empirical equation and its coefficients.
5. Calibrate the empirical coefficients based on the timing of liquefaction from the Stockwell transform and the Arias intensity-based liquefaction assessment curve. If the soil being used to develop the empirical relationship of the $\Sigma\Delta W/\sigma'_{vc} - r_u$ in Step 4 has different undrained cyclic behavior from the soil at the target site, the empirical coefficients should be calibrated to align with the timing of liquefaction from the Stockwell transform and the Arias intensity-based liquefaction curve.

Empirical Curve: $\Sigma\Delta W/\sigma'_{vc} - r_u$

The empirical relationship $\Sigma\Delta W/\sigma'_{vc} - r_u$ is critical to estimate r_u over time because the relationship directly converts the cumulative strain energy into r_u. This study developed empirical curves by extracting data from Kokusho and Kaneko (2018), who performed

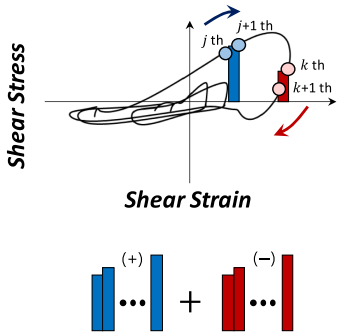

Fig. 5. Strain energy calculation for irregular loadings from stress–strain hysteresis loops.

$$r_u = \begin{cases} \left(\dfrac{\Sigma\Delta W/\sigma'_{vc}}{\Sigma\Delta W/\sigma'_{vc}+\alpha}\right) \Big/ \left(\dfrac{\beta}{\beta+\alpha}\right), & \Sigma\Delta W/\sigma'_{vc} < \beta \\ 1, & \Sigma\Delta W/\sigma'_{vc} \geq \beta \end{cases} \quad (8)$$

cyclic torsional shear tests for Futtsu beach sand [Figs. 6(a and b)]; circle symbols indicate the extracted data from Kokusho and Kaneko (2018), and solid lines represent the trend lines of the fitted curves developed using the extracted data in Figs. 6(a and b). The test parameters were the initial confining stress (σ'_{vc}) and D_r of the soil; σ'_{vc} was 49, 98, and 196 kPa, and D_r was 30% and 50%. Although previous literature applied different forms of the equation for the empirical equations (Jafarian et al. 2012; Ko and Kayen 2024), this study developed an empirical equation using two coefficients, α and β, to capture the slope of r_u development and the minimum required $\Sigma\Delta W/\sigma'_{vc}$ to liquefy the soil

where β = minimum normalized strain energy required for liquefaction triggering (capacity energy); and α = empirical coefficient, which defines a trend in the simulation of rate of pore pressure generation corresponding to the slope of the $\Sigma\Delta W - r_u$ curve. The $\Sigma\Delta W/\sigma'_{vc}$ required to trigger liquefaction ($r_u = 1$ increases with D_r because the soil becomes less contractive). The $\Sigma\Delta W/\sigma'_{vc}$ for the same r_u tends to be slightly lower as σ'_{vc} decreases, indicating that r_u develops faster for lower σ'_{vc} under the same $\Sigma\Delta W/\sigma'_{vc}$. Hence, the coefficient β is a function of D_r [Fig. 6(c)], whereas the coefficient α is a function of D_r and σ'_{vc} [Fig. 6(d)]. The values of β and α depend on the soil type. To estimate r_u responses at the depths of 3.44 and 7.44 m where the pore water pressure sensors UP1 and UP3 were installed, this study used β and α associated with average D_r values of 40% and 25%, respectively, as determined from the relative density profile [Fig. 3(b)]. The β and α for D_r of 40% and 25% were calculated through the empirical equations in Figs. 6(c and d). In this study, the use of limited laboratory test data established the relationship between β, α, D_r, and σ'_{vc}. However, in order to develop more elaborate empirical equations, supplementary laboratory test data are necessary.

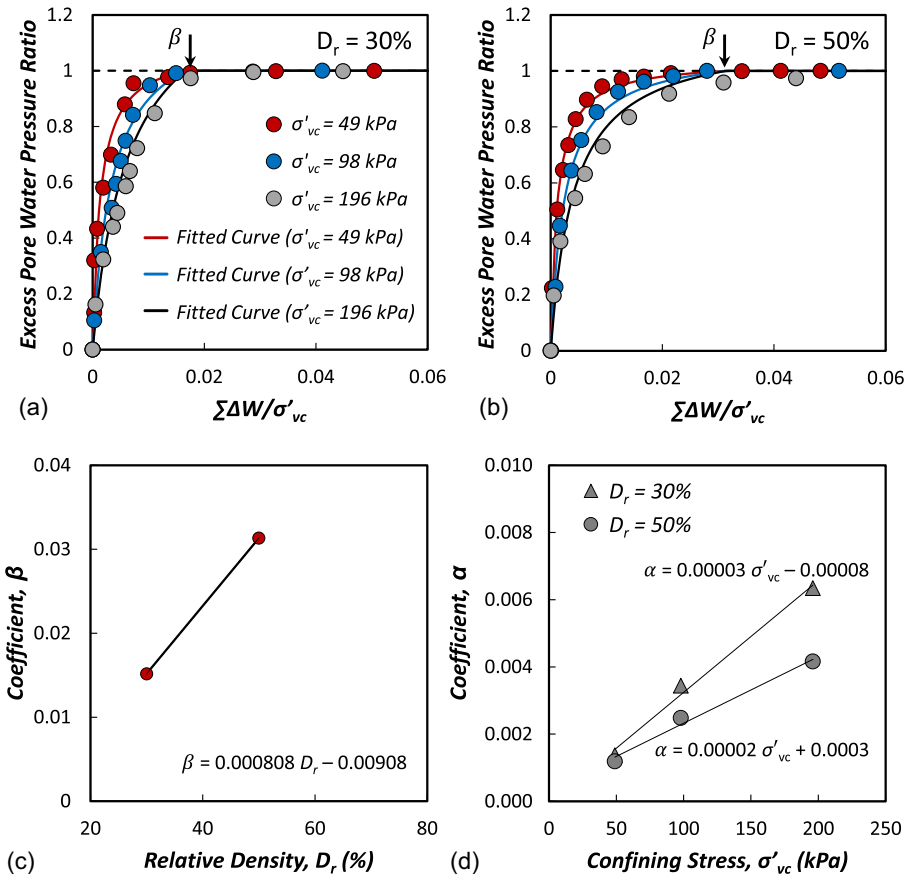

Fig. 6. Cyclic torsional shear test results performed by Kokusho and Kaneko (2018) and developed empirical equations: (a and b) excess pore water pressure ratio with normalized cumulative energy ($\Sigma\Delta W/\sigma'_{v0}$) for the relative density of 30% and 50%, respectively; (c) empirical coefficient β with the relative density (D_r); and (d) empirical coefficient α with the effective stress (σ'_{vc}) and D_r.

Bidirectional Shaking

Bidirectional shaking imposes more strain energy on soils and induces faster pore water pressure buildup than when one-dimensional shaking is applied to liquefiable soil (El Shafee et al. 2017). This study implemented four methods to calculate the cumulative strain energy from bidirectional shaking. The combined energy method estimates the strain energy of the soil by adding up the individually calculated energies for the two orthogonal horizontal components. Hence, $\tau - \gamma$ hysteresis loops should be estimated for each direction (Fig. 7), and the strain energies calculated using Eq. (7) for both are combined. Because the two orthogonal vectors, which correspond to the computed shear stress and strain, do not interfere with each other, the cumulative strain energies for each horizontal component represent the dissipated energy of the soil for that specific component. Hence, the combined energy calculated from the cumulative strain energies of the two orthogonal horizontal components represents the most reasonable measure of the strain energy that the liquefiable soil dissipates during bidirectional shaking (El Shafee et al. 2017).

The fundamental concept of the other three methods is to create an estimated equivalent acceleration record from the time histories of two orthogonal components. Three representative methods, RSS, RotD100, and geometric mean, combine acceleration time histories of two orthogonal components using Eqs. (9)–(11)

$$a_{\mathrm{RSS}}(t) = \sqrt{a_{EW}^2(t) + a_{NS}^2(t)} \tag{9}$$

$$a_{\mathrm{ROT}}(t,\theta) = a_{EW}(t) \cdot \cos(\theta) + a_{NS}(t) \cdot \sin(\theta) \tag{10}$$

$$a_{\mathrm{GeoMean}}(t) = \sqrt{|a_{NS}(t) \cdot a_{EW}(t)|} \tag{11}$$

where $a_{\mathrm{RSS}}(t)$ = root sum squared acceleration time history; $a_{EW}(t)$ and $a_{NS}(t)$ = recorded acceleration time histories in the E–W and N–S directions, respectively; $a_{\mathrm{ROT}}(t,\theta)$ = combined single-time history corresponding to an azimuth given by an increment of rotation angle, θ; $a_{\mathrm{GeoMean}}(t)$ = geometric mean acceleration time history of two orthogonal component time histories; and a_{RSS} = length of a vector of the two-horizontal acceleration. From the $a_{\mathrm{ROT}}(t,\theta)$, RotD100 (t) is estimated by obtaining the maximum acceleration over all rotation angles for each time step (Boore 2010).

The acceleration records from TA7, which was located in the As1 sand layer at a depth of 11.9 m, exemplify the combined time histories (Fig. 8). As shown in Fig. 8, the combined accelerations indicate positive acceleration responses over time. The PGAs of two horizontal motions were 0.13 and 0.15 g for the E–W and N–S directions, respectively. Meanwhile, the RSS method exhibited a higher PGA than the original records [PGA of $a_{\mathrm{RSS}}(t) =$ 0.16 g], whereas the PGA of the RotD100 was 0.15 g, similar to the PGA of the original record in N–S direction. The PGA of $a_{\mathrm{GeoMean}}(t)$ was 0.10 g, which is lower than that of the original records. The single time history corresponding to each method, RSS, RotD100, and GeoMean, was used to calculate the $\tau - \gamma$ and hysteretic responses turned into cumulative energy.

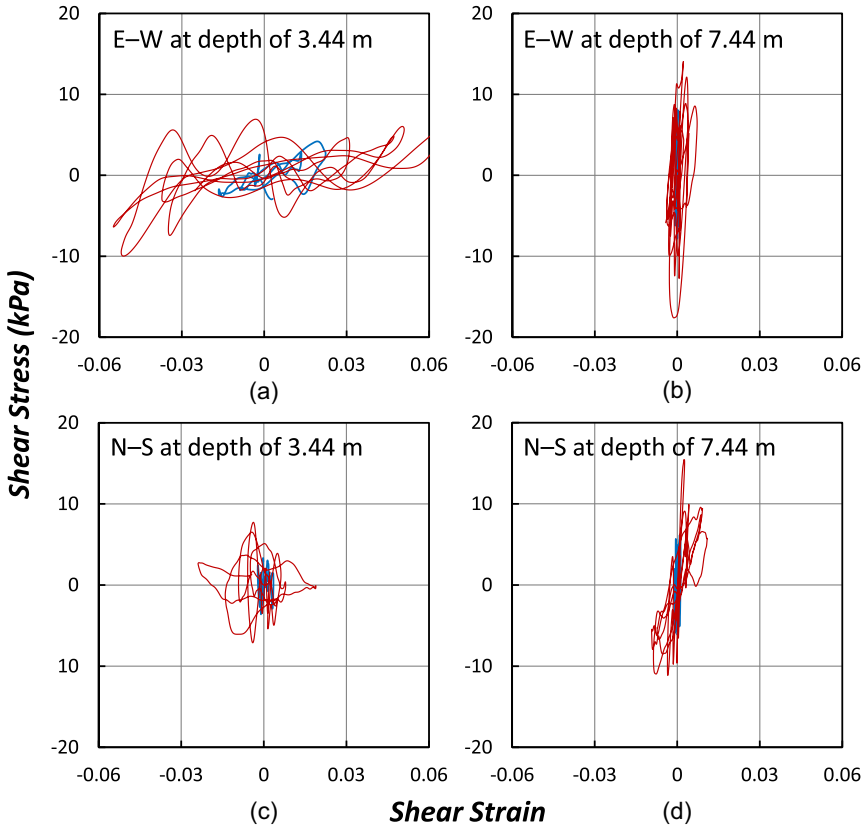

Fig. 7. Shear stress and shear strain hysteresis loops during the period corresponding to D5–75, which is the time difference between the 5% and 75% Arias intensity : (a) E–W direction at the depth of 3.44 m; (b) E–W direction at the depth of 7.44 m; (c) N–S direction at the depth of 3.44 m; and (d) N–S direction at the depth of 7.44 m.

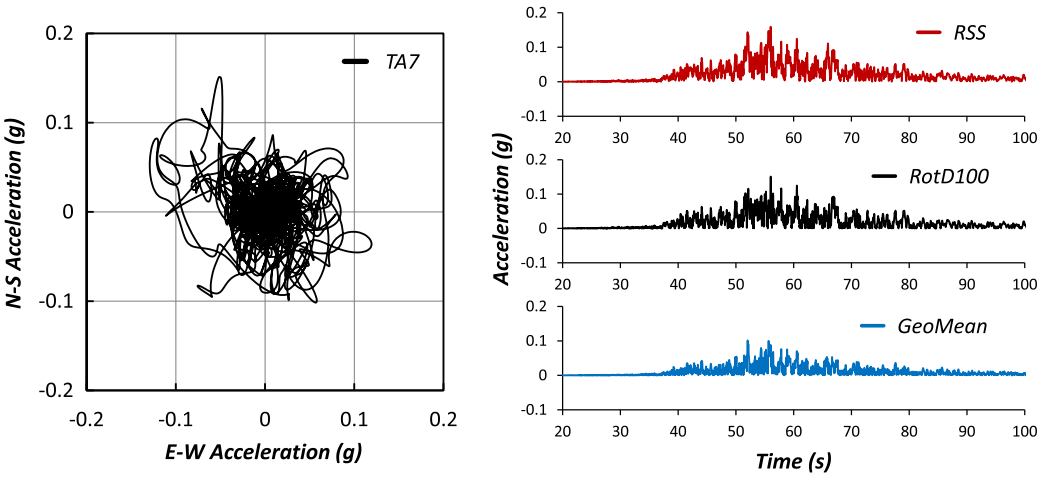

Fig. 8. Two horizontal motions and an equivalent motion of two horizontal motions of TA7: root sum squared, RotD100, and geometric mean.

Energy-Based Method for Soil Liquefaction Evaluation at the Port of Kushiro

Cumulative Strain Energy over Time ($\Sigma\Delta W/\sigma'_{vc}$) and Excess Pore Water Pressure Ratio

The four methods demonstrate a different pattern of cumulative energy over time at depths of 3.44 and 7.44 m, where the pore water pressure sensors UP1 and UP3 were installed (Fig. 9). The dotted lines represent the normalized cumulative energy corresponding to the r_u values of 0.1, 0.5, and 1.0. The dotted lines differ depending on the depth because the effective stress at that depth leads to different coefficients of α. For the depth of 3.44 m, the combined energy reaches first a $\Sigma\Delta W/\sigma'_{vc}$ of 0.00017 corresponding to the $r_u = 0.1$ at 42 s when the I_a of TA8 is about 3% of I_a (i.e., I_a will indicate the I_a from the TA8 record in this section). However, the other methods reveal slower timing of when the cumulative energy reaches the energy corresponding to $r_u = 0.1$ (e.g., the geometric mean reaches the cumulative energy corresponding to $r_u = 0.1$ at 52 s, which is 24% of I_a). The combined energy develops cumulative energy faster than using the other methods.

The cumulative energy buildup for the depth of 7.44 m exhibited the fastest energy buildup of the combined energy from when $r_u = 0.1$ to the end of the shaking. The timing of $r_u = 0.1$ and 0.5 was slower than the case of a depth of 3.44 m. As shown in Fig. 6, the shear stress of the soil at a depth of 3.44 m was lower than that of 7.44 m, but the shear strain was five times larger than that of 7.44 m for the case of the E–W direction [Figs. 7(a and b)]. The measured horizontal displacement at the backfill was more significant for the soil closer to the surface during the 2003 Tokachi-oki earthquake (Sasajima et al. 2004). This consequence may have affected the disparity in shear strain between the 3.44-m and 7.44-m cases. From 44 to 50 s, corresponding to 5% to 13% of I_a, the soil layer at a depth of 3.44 m developed more shear strain than that at 7.44 m. From 50 to 65.7 s, corresponding to 13% to 75% of I_a, however, the soil layer at a depth of 7.44 m exhibited more shear stress than that at 3.44 m. Accordingly, the cumulative energy buildup attributed to the area of the hysteresis loops was slower at a depth of 7.44 m compared to 3.44 m until approximately 50 s. However, at a depth of 7.44 m, most of the energy accumulated between 50 and 65.7 s.

The estimated r_u over time had the same trend as the cumulative energy buildup because Eq. (8) converted the cumulative energy into r_u. The energy-based method estimated the expected r_u buildup of UP1 and UP3 during the 2003 Tokachi-oki earthquake [Figs. 10(a and b)]. At UP1, the estimated response generated excess pore water pressure starting at 40 s, corresponding to 1% of I_a. The r_u was fully developed around 68 s, corresponding to 83.2% of I_a. The combined energy method only showed r_u exceeding 0.9, indicating the potential triggering of soil liquefaction at the 3.44-m soil layer. The methods using equivalent acceleration estimated r_u as less than 0.9 at the end of the shaking, which is an irrational result considering that the stress-based evaluation indicated the triggering of soil liquefaction at the Port of Kushiro. The estimated r_u at a depth of 7.44 m for UP3 demonstrated the same results irrespective of the methods, and the r_u buildup started

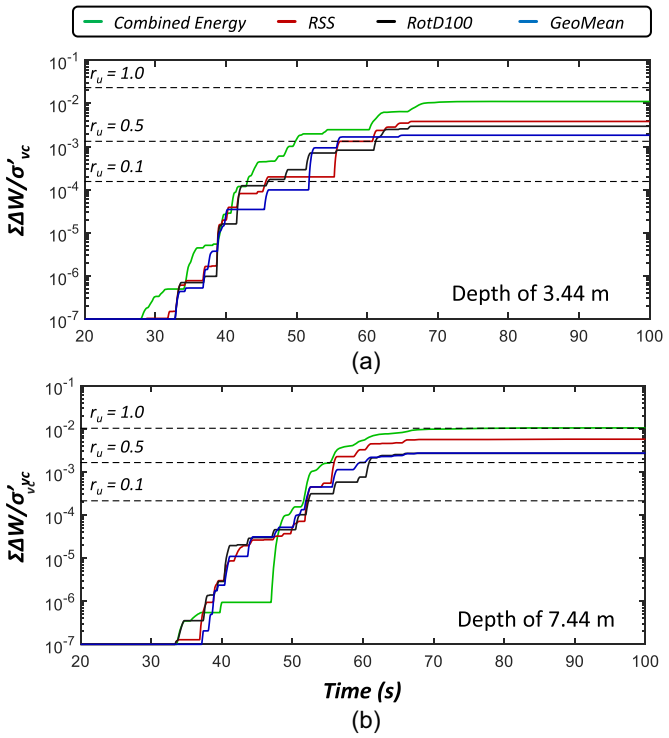

Fig. 9. Cumulative energy over time for four energy calculation methods: (a) depth of 3.44 m; and (b) depth of 7.44 m.

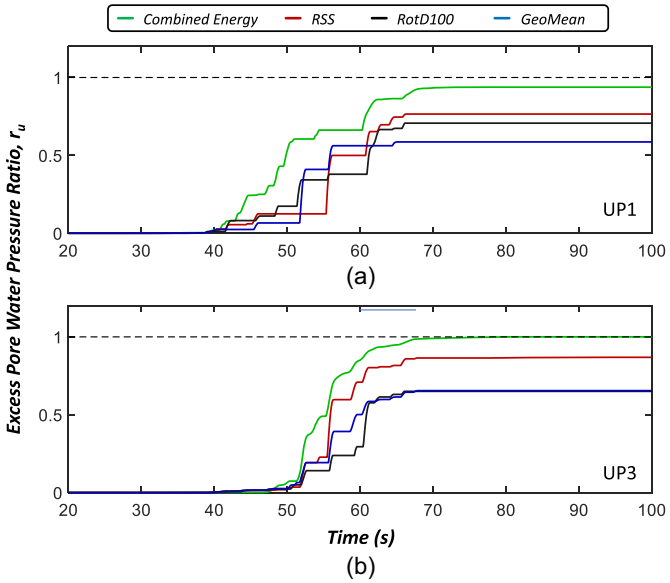

Fig. 10. Estimated excess pore water pressure ratio using energy-based method: (a) depth of 3.44 m, where the UP1 sensor was installed; and (b) depth of 7.44 m, where the UP3 sensor was installed.

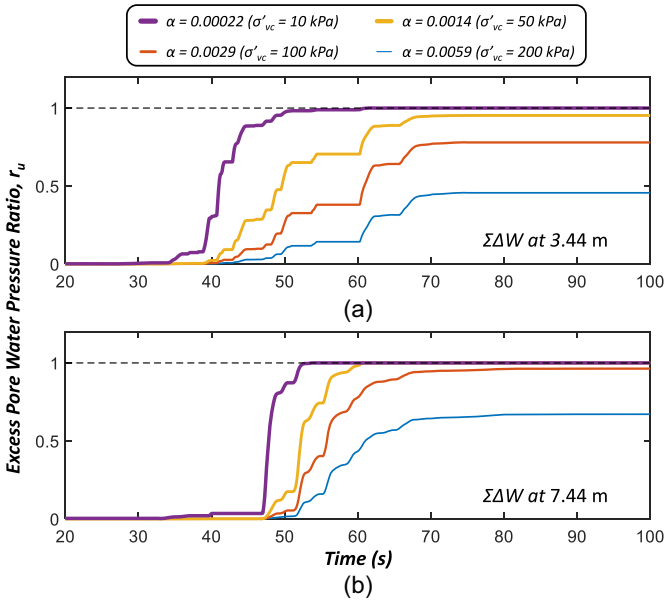

Fig. 11. Sensitivity analysis of coefficient α corresponding to the effective stress of 10, 50, 100, and 200 kPa: (a) the depth of 3.44 m; and (b) the depth of 7.44 m.

at approximately 48 s, corresponding to 9.2% of I_a. The estimated r_u for UP1 did not reach 1.0 (i.e., it reached 0.93 at 68 s), and that for UP3 showed the triggering of liquefaction at 67.6 s for the combined energy. However, the timing of liquefaction is sensitive to the coefficient α. The following section discusses the sensitivity analysis of α for the energy-based method.

Sensitivity Analysis of Coefficient α

The coefficient α in Eq. (8) affects how much $\Sigma\Delta W/\sigma'_{vc}$ is required to reach a certain level of r_u before liquefaction; that is, the coefficient α has an influence on the excess pore pressure buildup. Because α is a function of the effective stress of the soil, a suite of α for sensitivity analysis was made by varying the effective stress. The values of α for the sensitivity analysis corresponded to the effective stress of 10, 50, 100, and 200 kPa. The value of $\Sigma\Delta W$, which was calculated by the combined energy method, at depths of 3.44 and 7.44 m was used to evaluate the effect of α on the estimation of r_u buildup during the 2003 Tokachi-oki earthquake (Fig. 11). The larger the effective stress, the more energy is required to liquefy the soil, so the r_u buildup becomes faster as α decreases. For the depth of 3.44 m, the soil liquefaction was triggered only for the cases of using α corresponding to 10 kPa. The case of using α corresponding to 10 kPa demonstrated the timing of liquefaction around 50 s, whereas the other cases delayed the timing of liquefaction or did not manifest liquefaction [Fig. 11(a)]. The case for the depth of 7.44 m showed a consistent result with the previous case [Fig. 11(b)]. This case showed, however, two estimations that reached $r_u = 1$ because $\Sigma\Delta W$ was already close enough to β after being normalized by the effective stress. Consequently, α can adjust the timing of liquefaction for the energy-based method, and α should be calibrated if the timing of liquefaction from the energy-based method does not match with the Stockwell transform.

Evaluation of the Timing of Liquefaction

The energy-based soil liquefaction method estimates different timing of liquefaction triggering if the soil used to develop the correlation curve between $\Sigma\Delta W/\sigma'_{vc}$ and r_u differs from the soil at the site of interest. In this case, the timing of liquefaction should be cross-checked by comparing it with that from the time-frequency responses and the Arias intensity-based soil liquefaction evaluation curve.

Time-Frequency Response of Liquefied Soil Layer

Liquefaction is accompanied by cumulative cyclic strain and the reduction of the effective stress, and it leads to the reduction of V_s, which is a function of effective stress. The fundamental site frequency (f_n) decreases according to the reduced V_s during the soil liquefaction (Millen et al. 2021; Özener et al. 2020), and the Stockwell transform, which evaluates the time-frequency responses of the acceleration records, demonstrates the change of f_n during the earthquake (i.e., $f_n = V_s/4H$; H is the depth of the soil site). Many case histories demonstrated the reduction of f_n at the liquefied site through the Stockwell transform (Kostadinov and Yamazaki 2001; Unjoh et al. 2012). However, some components of the change of f_n are also affected by the changes in the frequency content of the earthquake motion (Kramer et al. 2016). In order to isolate the genuine changes of f_n over time, this study computed the ratio of the horizontal Stockwell transforms using two acceleration records. Such ratio plots illustrate the transfer function of the soil layers sandwiched between the two accelerometers. To investigate the timing of liquefaction at 3.44 and 7.44 m, two sets were used: one using UA5 and UA6 and another employing UA6 and TA7 to calculate the ratio of the Stockwell transforms.

In order to consider both horizontal motions in a single Stockwell transform plot, this study computed the horizontal power spectrogram $[P_H(t,f)]$ by combining the norms of the E–W and N–S directions' power spectrograms, as follows:

$$P_H(t,f) = [\mathrm{Re}\,(S_{EW}(t,f))]^2 + [\mathrm{Im}(S_{EW}(t,f))]^2 + [\mathrm{Re}\,(S_{NS}(t,f))]^2 + [\mathrm{Im}(S_{NS}(t,f))]^2 \quad (12)$$

where $S_{EW}(t,f)$ and $S_{NS}(t,f)$ = Stockwell transforms of the E–W and N–S directions, respectively; and Re() and Im() = real and imaginary components of Stockwell transforms. For instance,

the ratio of the horizontal Stockwell transforms using UA5 and UA6 was calculated as $P_{H_{UA5}}(t,f)/P_{H_{UA6}}(t,f)$.

The acceleration data from UA5, UA6, and TA7 were used to compute the Stockwell transform of horizontal motions and the ratio of the horizontal Stockwell transforms (Fig. 12). The ratio plots illustrate the degree of amplification at each frequency over time [Figs. 12(c and f)]. The horizontal Stockwell transforms of UA5, UA6, and TA7 revealed lower frequencies, particularly around 0.4 Hz after 55 s [Figs. 12(a, b, d, and e)]. The average V_s and the height of the layer between UA5 and UA6 were calculated as 136.26 m/s and 5.44 m, respectively. The calculated f_n ($= V_s/4H$) was 6.26 Hz, which aligns with the f_n observed in the ratio spectrum at 40 s before liquefaction [Fig. 12(c)]. For the layer between UA6 and TA7, the average V_s and the height of the layer were 111.62 m/s and 6.5 m, respectively, and the calculated f_n was 4.29 Hz, which corresponds to the f_n observed in the ratio spectrum at 40 s before the liquefaction [Fig. 12(f)]. Consequently, the ratio spectra clearly depict the transfer functions of the soil layers and the changes in f_n over time. The ratio spectra between UA5–UA6 and UA6–TA7 indicated changes in f_n beginning at approximately 50 s and around 54 s, respectively [Figs. 12(c and f)]. Therefore, the Stockwell transform spectra suggest that the liquefaction was triggered first in the soil layer between UA5 and UA6, followed by liquefaction in the layer between UA6 and TA7. In other words, based on the Stockwell transforms, the timing at 3.44 m (above UA6) is estimated to be under 50 s, whereas the timing of liquefaction at 7.44 m (above TA7 and below UA6) is estimated to be after 50 s.

Arias Intensity Curve

The Arias intensity I_a features scalar energy measures of ground motions and incorporates the amplitude, frequency components, and duration of the ground motion, such that the effect of bidirectional shaking on liquefaction can be reflected by the added Arias intensity (I_{hb}) of the two horizontal components of I_a. Kayen and Mitchell (1997) proposed the Arias intensity-based liquefaction assessment of soil deposits during earthquakes. The I_{hb} versus $(N_1)_{60}$ defined a clear boundary between liquefied and nonliquefied sites. This study used a boundary for a fines content of 15% proposed by Kayen and Mitchell (1997) [Figs. 13(a and c)]. The use of I_{hb} versus $(N_1)_{60}$ curve facilitates the identification of the timing of liquefaction because the Arias intensity is a time-dependent value.

The greatest energy buildup of I_a for the N–S and E–W (dotted blue lines) directions for UA6 and TA7 occurred between 40 and 60 s, and the I_{hb}s of UA6 and TA7 were 3.25 and 1.41 m/s at the end of the shaking, respectively. When it comes to the liquefaction boundary curve, the I_{hb} at the end of the shaking was located above the curve corresponding to $(N_1)_{60}$ at the depth where the UA6 and TA7 are installed. This implies that the site was significantly liquefiable under the 2003 Tokachi-oki earthquake. Meanwhile, liquefaction at the site should be triggered when I_a overlies the boundary curve; the curve elucidates the triggering of liquefaction at the site when I_{hb} reaches 0.27 and 0.48 m/s for the depth where UA6 and TA7 are installed. The retraced timing of triggering according to the liquefaction boundary curve was 48.7 s for UA6 and 55.0 for TA7 [Figs. 13(b and d)], which is comparable with the result from the Stockwell transform. Because seismic waves propagate upward from the bottom soil layer, the timing of liquefaction at 7.44 m (above TA7 and below UA6) was estimated to be after 55.0 s, whereas the timing at 3.44 m (above UA6) was estimated to be under 48.7 s.

Calibrated Excess Pore Water Pressure Ratio

The estimation of excess pore water pressure for UP1 and UP3 was calibrated by adjusting α so as to have a consistency of timing of liquefaction from the Stockwell transform and the Arias intensity-based soil liquefaction. The calibrated α was equal to 0.000052 and 0.00022 based on the fact that the timing of liquefaction occurred at 48.7 and 55.0 s at depths of 5.44 and 11.94 m where UA6 and TA7 were situated; the previous α values for UP1 and UP3 were 0.0016

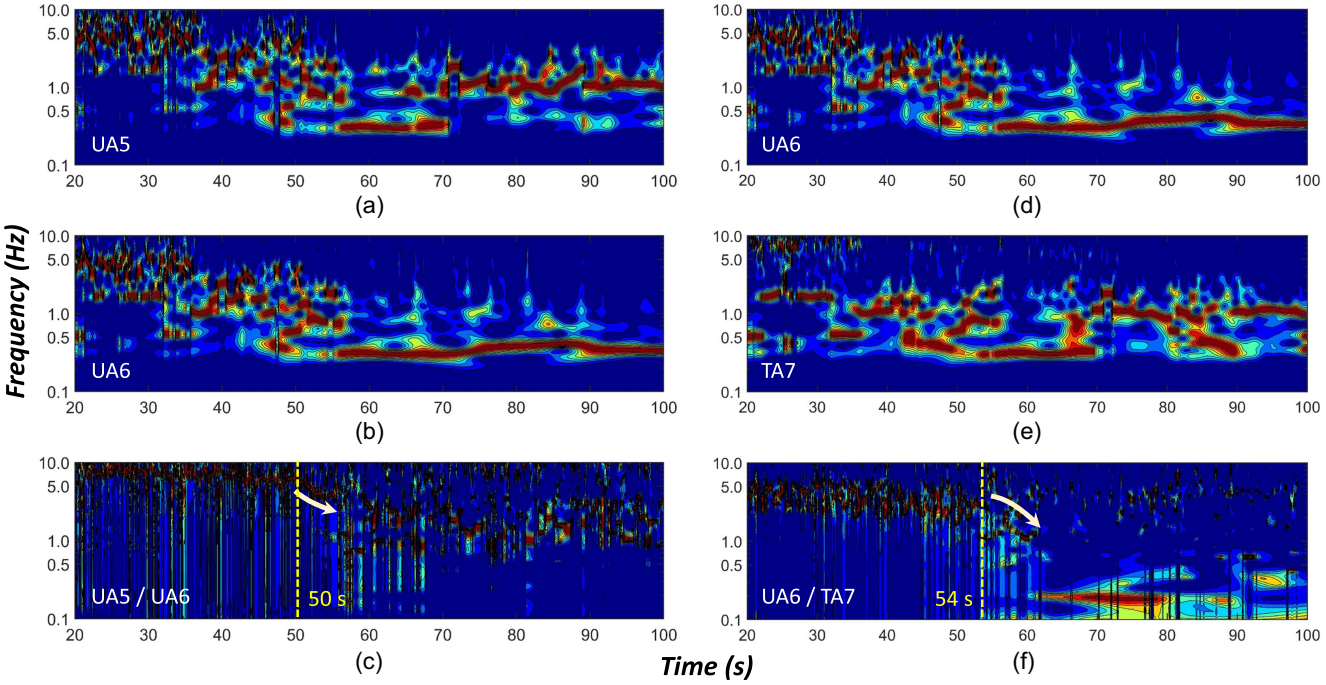

Fig. 12. Stockwell transforms for the acceleration record and the ratio of the Stockwell transforms: (a) horizontal motion (UA5); (b) horizontal motion (UA6); (c) ratio between UA5 and UA6; (d) horizontal motion (UA6); (e) horizontal motion (TA7); and (f) ratio between UA6 and TA7.

J. Geotech. Geoenviron. Eng., 2024, 150(10): 05024010

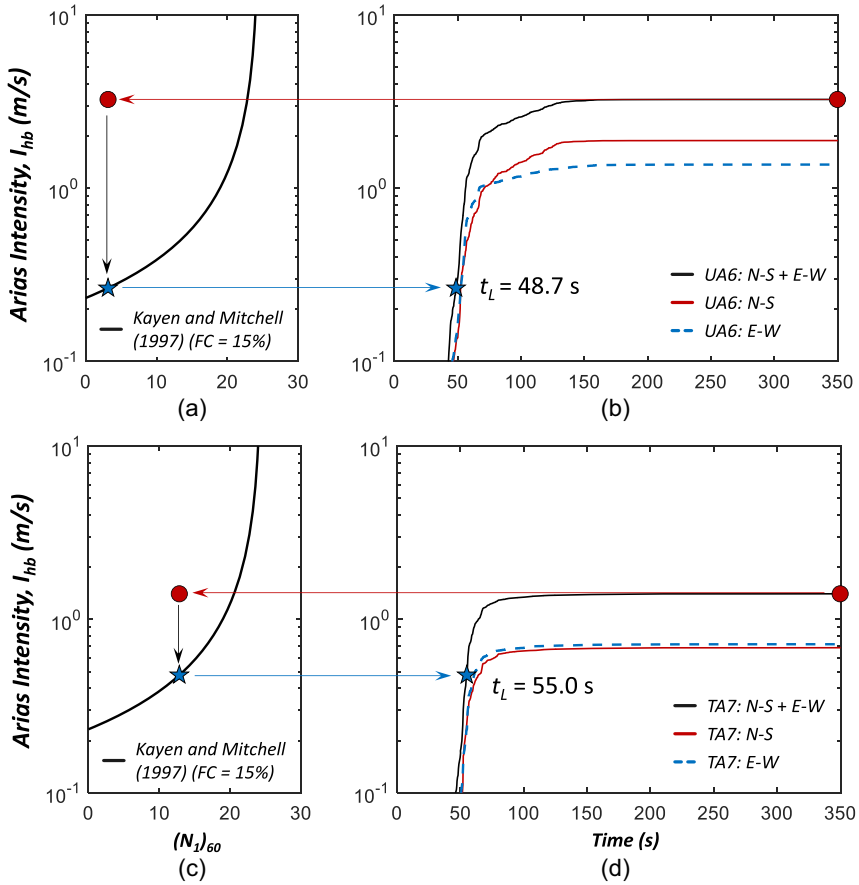

Fig. 13. Arias intensity–based soil liquefaction evaluation: (a) Arias intensity versus $(N_1)_{60}$ curve for a fines content of 15% for UA6; (b) Arias intensity time histories of UA6 for two horizontal motions; (c) Arias intensity versus $(N_1)_{60}$ curve for a fines content of 15% for TA7; and (d) Arias intensity time histories of TA7 for two horizontal motions. [Data for (a and c) from Kayen and Mitchell 1997.]

and 0.0024, respectively. Using the cumulative combined energy ($\Sigma\Delta W$) for each depth where UP1 and UP3 were installed, the excess pore water pressure ratio for UP1 and UP3 was re-evaluated according to the calibrated α (Fig. 14). For the UP1 case, r_u exceeded 0.95, around 48.7 s. The r_u of UP3 abruptly developed from 47 to 53 s and reached $r_u > 0.95$ around 55 s. Overall, those calibrated estimations demonstrated more rational results of r_u buildup rather than the recorded responses, as shown in Figs. 2(e and g).

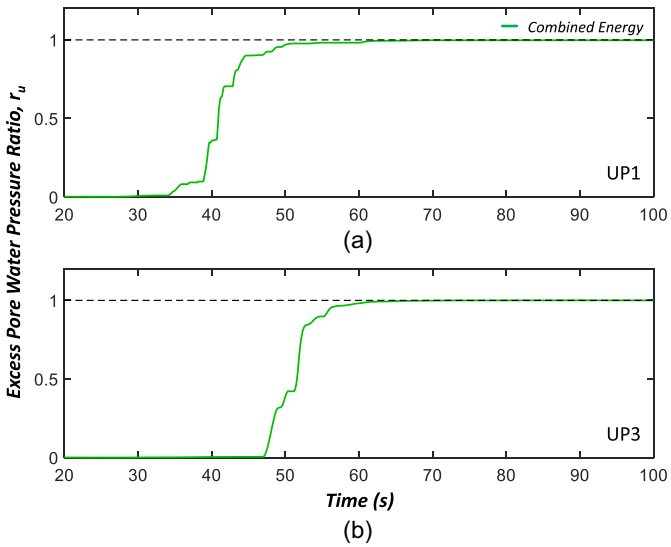

Fig. 14. Estimated excess pore water pressure ratio over time based on the cumulative energy using combined energy: (a) UP1; and (b) UP3.

Discussion and Limitations

Comparison of Empirical Relationships between $\Sigma\Delta W/\sigma'_{vc} - r_u$

The estimation of r_u depends on empirical relationships between $\Sigma\Delta W/\sigma'_{vc} - r_u$. The Green, Mitchell, and Polito (GMP) model (Green 2001) and the model developed by Jafarian et al. (2012) were used to evaluate the r_u buildup at the backfill of the Kushiro port depending on the empirical relationships. The fitted curves developed in this study are compared with the GMP model in Figs. 15(a and b). The GMP model for a confining stress of 98 kPa has a similar value of β, the normalized cumulative energy ($\Sigma\Delta W/\sigma'_{vc}$) corresponding to $r_u = 1$ for both 30% and 50% relative density. In terms of the trend of r_u buildup, the GMP model for a confining stress of 196 kPa aligns more closely with the fitted curves. Because the GMP model was developed using Monterey No. 0/30 sand, Yatesville sand, and Yatesville silty sand (Polito et al. 2008), the model generally exhibits a different relationship with the fitted curves.

Jafarian et al. (2012) developed a simple pore water pressure model based on cyclic torsional test results using Toyoura sand. Jafarian et al. (2012) described the empirical relationship between

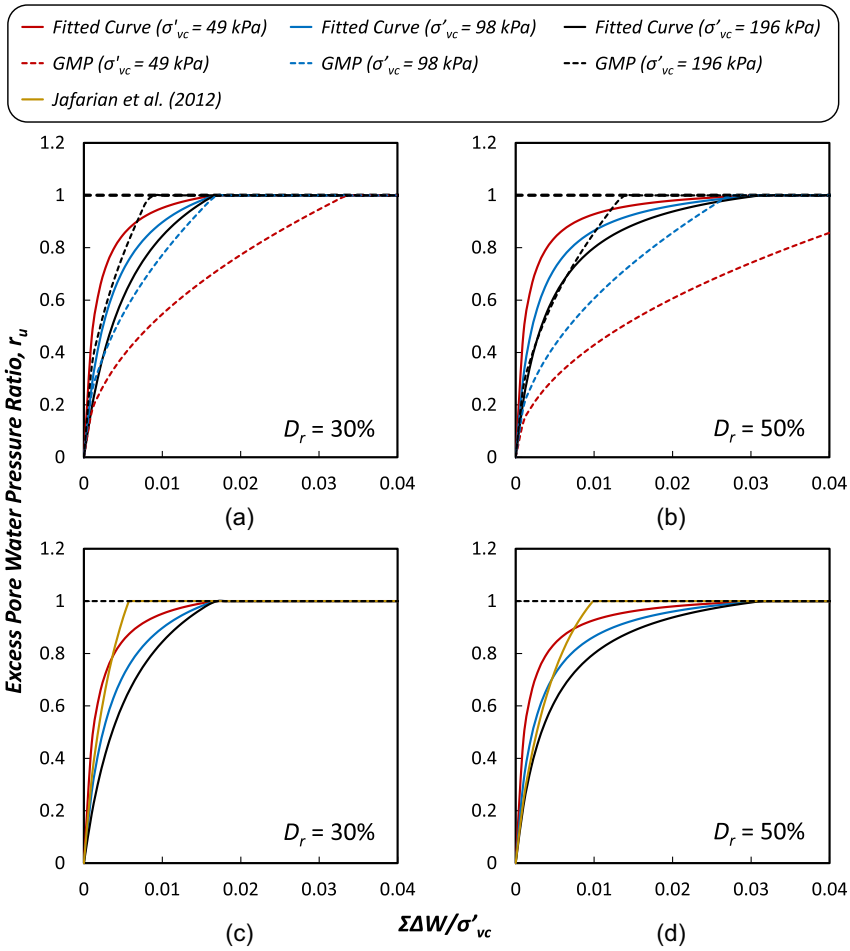

Fig. 15. Comparison of $\Sigma\Delta W/\sigma'_{vc}$–$r_u$ relationships obtained from fitted curves using Kokusho and Kaneko (2018) in Fig. 6, GMP model (Green 2001), and Jafarian et al. (2012): (a) relative density of 30% for the fitted curves and GMP model; (b) relative density of 50% for the fitted curves and GMP model; (c) relative density of 30% for the fitted curves and Jafarian et al. (2012); and (d) relative density of 50% for the fitted curves and Jafarian et al. (2012).

$\Sigma\Delta W/\sigma'_{vc} - r_u$ as a function of D_r [Figs. 15(c and d)]. The model developed by Jafarian et al. (2012) demonstrates a similar trend of r_u buildup, whereas the energy capacity corresponding to $r_u = 1$ is less than the β obtained from the fitted curves. Both Jafarian et al. (2012) and the GMP model show that the energy capacity required to liquefy the soil increases with D_r.

Both methods demonstrate different estimated r_u for UP1 and UP3 (Fig. 16). Because the model developed by Jafarian et al. (2012) has similar r_u trend with $\Sigma\Delta W/\sigma'_{vc}$, but with a smaller energy capacity of soil corresponding to $r_u = 1$ compared to the fitted curves, the model shows a similar r_u buildup when considering the combined energy from Fig. 10. However, it indicates liquefaction triggering for UP1 and an earlier timing of liquefaction for UP3. Meanwhile, as shown in Fig. 15, the GMP model exhibits a larger energy capacity as the confining stress decreases, resulting in a delayed r_u buildup and lower r_u values by the end of the earthquake. Accordingly, the estimated r_u is strongly affected by the choice of the model curve associated with $\Sigma\Delta W/\sigma'_{vc} - r_u$ relationships.

Arias Intensity: Comparison between Total Stress and Effective Stress Analysis

Kayen and Mitchell (1997) collected strong-motion records measured at the surface to develop Arias intensity-based liquefaction triggering curves. Given that the critical layers where liquefaction occurred in case histories were located at depth, they used total stress site response analyses to derive a depth reduction factor for Arias intensity. This factor is defined as the ratio of buried to surface cumulative Arias intensity. This study employed the curve to estimate the timing of liquefaction based on the measured acceleration responses, which were likely affected by pore water pressure buildup. Therefore, it is necessary to investigate the Arias intensity difference between nonlinear effective stress analysis and total stress analysis because the total stress analysis does not account for pore water pressure buildup.

The total stress analysis was conducted using the soil layer information for the nonlinear analysis in Table 1 (Fig. 17). The acceleration responses of the total stress analysis were comparable to those of the nonlinear analysis [Fig. 17(a)] until r_u is fully developed at approximately 56 s [Fig. 17(b)]. Beyond 56 s, these two acceleration responses diverged, leading to a disparity in cumulative Arias intensity. If the soil liquefies, it would lose its shear stiffness ($G \approx 0$), resulting in reduced acceleration responses due to site softening. In other words, the acceleration response from the total analysis is similar to that from the nonlinear analysis before liquefaction is triggered in the soil layer. The Arias intensity clearly illustrates the impact of soil liquefaction [Fig. 17(c)]; Arias intensities obtained from the total and nonlinear analyses are similar to each other before liquefaction triggering, but discrepancies emerge afterward. Consequently, employing Arias intensity curves

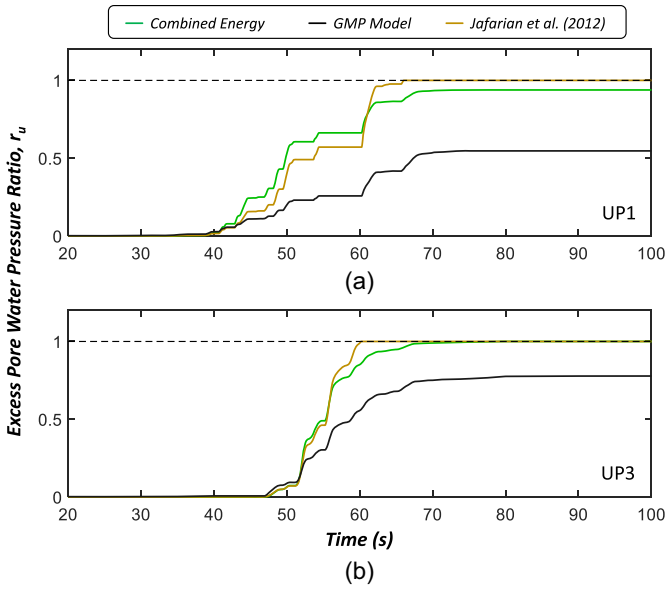

Fig. 16. Estimated excess pore water pressure ratio using combined energy, GMP model (Green 2001), and Jafarian et al. (2012): (a) depth of 3.44 m, where the UP1 sensor was installed; and (b) depth of 7.44 m, where the UP3 sensor was installed.

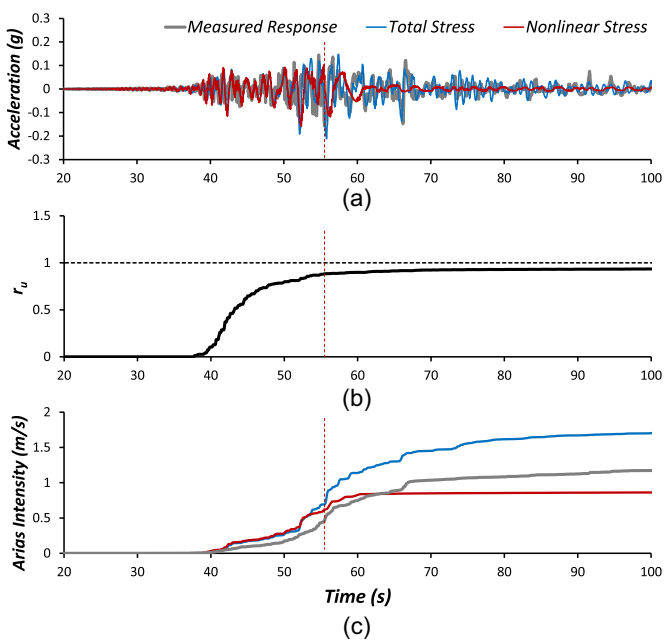

Fig. 17. Comparison between nonlinear effective stress and total stress analysis of the fifth layer (4.73–5.72 m depth) in E–W directions: (a) acceleration responses; (b) excess pore water pressure ratio from nonlinear effective stress analysis; and (c) and Arias intensity over time.

to determine the timing of liquefaction through the measured acceleration responses is a valid approach.

Uncertainties and Limitations

The method introduced in this study incorporates laboratory test results into the development of the empirical $\Sigma\Delta W/\sigma'_{vc} - r_u$ relationship for field applications, which gives rise to inherent uncertainties and limitations associated with the method. Several factors can affect laboratory test results. Regarding sample preparation, Jafarian et al. (2012) analyzed numerous results from cyclic triaxial, simple shear, and hollow cylinder torsional tests conducted using different sample preparation methods. They concluded that the method of sample preparation did not significantly alter the general trend of the $\Sigma\Delta W/\sigma'_{vc} - r_u$ relationship. Regarding test types, such as torsional shear, cyclic simple shear, and triaxial tests, Polito et al. (2013) found that the $\Sigma\Delta W/\sigma'_{vc}$ corresponding to the initiation of liquefaction were similar for cyclic triaxial and simple shear tests. Conversely, Polito (2017) revealed a significant difference in pseudo energy capacity (PEC) values, with cyclic simple shear tests showing a factor of 8.9 difference compared to cyclic triaxial tests. This difference might have been influenced by the relative volumes of the two specimen types but warrants further discussion in future studies.

To estimate r_u using the energy-based liquefaction method, vertically aligned accelerometers should be employed to capture the shear stress–strain responses of the soil layer between these accelerometers. These shear stress–strain responses using acceleration records assumes a shear beam behavior of liquefied soil, but the assumed shear beam response cannot properly capture the response of a complex soil profile, which is a limitation of the method. This limitation restricts the application to sites where vertical acceleration data have been recorded. Additionally, within the context of energy-based soil liquefaction evaluation, when applied energy exceeds the energy capacity of a particular soil layer, any excess energy must be redistributed to other soil layers that have not liquefied yet (Kokusho 2013). This process accounts for the redistribution of energy within the soil layers. In this study, the soil layers in the backfill were divided into two distinct layers, and the stress–strain responses of each layer were computed using UA5, UA6, and TA7. As illustrated by the cumulative energy over time (Fig. 9), the cumulative strain energies at depths of 3.44 and 7.44 m did not exceed the capacity corresponding to $r_u = 1$. This implies that the applied energy was effectively dissipated by the segmented soil layers.

Due to the lack of laboratory test parameters related to relative density, confining stress, and soil types, this study calibrated α based on the Stockwell transforms and Arias intensity-based triggering curves. However, the α and β parameters depend on accurate and sophisticated laboratory test results specific to the soil conditions at the field site of interest, which should be discussed in detail in a future study.

Conclusions

The 2003 Tokachi-oki earthquake caused soil liquefaction at the Port of Kushiro in Hokkaido. The installed excess pore water pressure transducers at the site malfunctioned, and the pore water pressure transducers recorded irrational responses such as a constant increase of r_u even after the end of the shaking and nonfluctuating responses during the shaking, amongst other issues. This study applied energy-based liquefaction evaluation to estimate the excess pore water pressure ratio from the acceleration records at the site in the Port of Kushiro. Three acceleration records were used to obtain the shear stress–strain hysteresis loops of the soil layers. The strain energy calculated by the hysteresis loops was converted into the excess pore water pressure using the empirical correlation between normalized cumulative energy and r_u. Moreover, the estimated excess pore water pressure was adjusted based on the timing of liquefaction derived from the Stockwell transform and Arias

intensity-based soil liquefaction curve. The main findings of this study are summarized as follows:

1. One-dimensional equivalent linear site response analyses and the simplified method were conducted to calculate the applied cyclic stress ratio at the backfill of the Port of Kushiro during the 2003 Tokachi-oki earthquake. The cyclic resistance ratio obtained from $(N_1)_{60}$ estimated the factor of safety at the site, and the stress-based method indicated that the site would experience severe liquefaction during the earthquake.
2. The empirical relationship between the normalized cumulative energy and r_u is necessary to perform energy-based soil liquefaction evaluation. This study developed an empirical equation using two coefficients, α and β, which are a function of the initial confining stress and the relative density of the soil, respectively. The developed empirical equation showed that more energy was required to liquefy the soil as the relative density and confining stress increased.
3. Four different methods were used to consider the effect of the bidirectional shaking of the earthquake. Three methods combined two horizontal motions into an equivalent motion and calculated strain energy. Meanwhile, the combined method obtained the strain energy by summing the individually calculated energy from two horizontal motions. The three methods combining two horizontal motions were insufficient for evaluating energy-based liquefaction problems in terms of r_u development.
4. The rate of excess pore water pressure buildup is sensitive to the coefficient α, so a sensitivity analysis of α was conducted. The result showed that the lower α corresponding to the lower confining stress caused the faster r_u buildup.
5. Because the soil for developing the empirical relationship differed from the soil at the Port of Kushiro, the timing of liquefaction was adjusted based on the Stockwell transform and Arias intensity-based liquefaction assessment curve. The Stockwell transform and Arias intensity-based liquefaction assessment estimated comparable timing of liquefaction at the site. As a result, the excess pore water pressure was calibrated by calibrating the α parameter leading to a reasonable estimate of the r_u buildup at the Port of Kushiro during the 2003 Tokachi-oki earthquake based on the energy-based method.

Appendix. Confining Stress Dependency of Cumulative Strain Energy

Cyclic resistance ratio (τ/σ'_{vc}) for the stress-based liquefaction evaluation tends to decrease as the confining stress (σ'_{vc}) increases. However, the normalized cumulative strain energy $(\Sigma\Delta W/\sigma'_{vc})$ tends to increase with σ'_{vc}. Here, the σ'_{vc} dependency of $\Sigma\Delta W/\sigma'_{vc}$ is verified through the $\tau-\gamma$ hysteresis loop.

For the idealized $\tau-\gamma$ hysteresis loop, $\tau-\gamma$ relationship can be expressed as the hyperbolic model, as follows (Kokusho 2017):

$$\tau = G_{\max}\gamma_r \frac{(\gamma/\gamma_r)}{1+(\gamma/\gamma_r)} = G_{\max}\gamma_r f(\gamma/\gamma_r) \tag{13}$$

where $G_{\max}$ = initial shear modulus; and γ_r = reference shear strain for $G/G_{\max} = 0.5$ in the hyperbolic model.

Meanwhile, the dissipated energy can be expressed as follows:

$$\Delta W = \oint \tau d\gamma \tag{14}$$

Using Eqs. (13) and (14), the normalized cumulative strain energy is calculated as follows:

$$\begin{aligned}\Delta W/\sigma'_{vc} &= \left(\oint \tau d\gamma\right)\Big/\sigma'_{vc} \\ &= \frac{G_{\max}\gamma_r}{\sigma'_{vc}}\oint f(\gamma/\gamma_r)d\gamma \\ &= \frac{G_{\max}\gamma_r^2}{\sigma'_{vc}}\oint f(\gamma/\gamma_r)d(\gamma/\gamma_r)\end{aligned} \tag{15}$$

$G_{\max}$ is a function of σ'_{vc}, as follows:

$$G_{\max} = G_0 \times (\sigma'_{vc}/P_a)^{0.5} \tag{16}$$

where G_0 = shear modulus at 1 atm, P_a. In the hyperbolic model, γ_r is defined as (Kokusho 2017)

$$\gamma_r = \tau_f/G_{\max} = \frac{\sigma'_{vc}\tan\phi}{G_0\times(\sigma'_{vc}/P_a)^{0.5}} = \frac{(\sigma'_{vc}/P_a)^{0.5}}{G_0/P_a}\tan\phi \tag{17}$$

where τ_f = ultimate shear strength; and ϕ = internal friction angle. Using Eqs. (16) and (17), Eq. (15) can be rearranged as follows:

$$\begin{aligned}\Delta W/\sigma'_{vc} &= \frac{G_0\times(\sigma'_{vc}/P_a)^{0.5}}{\sigma'_{vc}}\left[\frac{(\sigma'_{vc}/P_a)^{0.5}}{G_0/P_a}\tan\phi\right]^2 \\ &\quad\times\oint f(\gamma/\gamma_r)d(\gamma/\gamma_r) \\ &= \frac{\tan^2\phi}{G_0/P_a}(\sigma'_{vc}/P_a)^{0.5}\oint f(\gamma/\gamma_r)d(\gamma/\gamma_r)\end{aligned} \tag{18}$$

Eq. (18) implies that $\Delta W/\sigma'_{vc}$ tends to increase in proportion to the square root of the σ'_{vc} for the same soil. In other words, $\Delta W/\sigma'_{vc}$ is normalized in terms of physical dimensions but not numerically because $\Delta W/\sigma'_{vc}$ is still influenced by σ'_{vc}. Therefore, for the given r_u, a larger $\Delta W/\sigma'_{vc}$ is required as the σ'_{vc} increases.

Data Availability Statement

Some or all data, models, or code that support the findings of this study are available from the corresponding author upon reasonable request.

Acknowledgments

The authors thank the Hokkaido Regional Development Bureau, Ministry of Land, Infrastructure, Transport and Tourism, Japan, for providing the data used in this study.

References

Bartlett, S. F., and T. L. Youd. 1995. "Empirical prediction of liquefaction-induced lateral spread." *J. Geotech. Eng.* 121 (4): 316–329. https://doi.org/10.1061/(ASCE)0733-9410(1995)121:4(316).

Boore, D. M. 2010. "Orientation-independent, nongeometric-mean measures of seismic intensity from two horizontal components of motion." *Bull. Seismol. Soc. Am.* 100 (4): 1830–1835. https://doi.org/10.1785/0120090400.

Boulanger, R. W., and I. M. Idriss. 2014. *CPT and SPT based liquefaction triggering procedures*. Rep. No. UCD/CGM-14/01. Davis, CA: Univ. of California.

CEN (European Committee for Standardization). 2004. *Eurocode 8—Design of structures for earthquake resistance. Part 5: Foundations, retaining structures and geotechnical aspects*. EN 1998-5:2004. Brussels, Belgium: CEN.

Cetin, K. O., and H. T. Bilge. 2012. "Performance-based assessment of magnitude (duration) scaling factors." *J. Geotech. Geoenviron.*

Eng. 138 (3): 324–334. https://doi.org/10.1061/(ASCE)GT.1943-5606.0000596.

Cetin, K. O., and R. B. Seed. 2004. "Nonlinear shear mass participation factor (RD) for cyclic shear stress ratio evaluation." *Soil Dyn. Earthquake Eng.* 24 (2): 103–113. https://doi.org/10.1016/j.soildyn.2003.10.008.

Cetin, K. O., R. B. Seed, R. E. Kayen, R. E. S. Moss, H. T. Bilge, M. Ilgac, and K. Chowdhury. 2018a. "SPT-based probabilistic and deterministic assessment of seismic soil liquefaction triggering hazard." *Soil Dyn. Earthquake Eng.* 115 (Dec): 698–709. https://doi.org/10.1016/j.soildyn.2018.09.012.

Cetin, K. O., R. B. Seed, R. E. Kayen, R. E. S. Moss, H. T. Bilge, M. Ilgac, and K. Chowdhury. 2018b. "The use of the SPT-based seismic soil liquefaction triggering evaluation methodology in engineering hazard assessments." *MethodsX* 5 (Apr): 1556–1575. https://doi.org/10.1016/j.mex.2018.11.016.

Davis, R. O., and J. B. Berrill. 1982. "Energy dissipation and seismic liquefaction in sands." *Earthquake Eng. Struct. Dyn.* 10 (1): 59–68. https://doi.org/10.1002/eqe.4290100105.

El Shafee, O., T. Abdoun, and M. Zeghal. 2017. "Centrifuge modelling and analysis of site liquefaction subjected to biaxial dynamic excitations." *Géotechnique* 67 (3): 260–271. https://doi.org/10.1680/jgeot.16.P.049.

FEMA. 2009. *Recommended seismic provisions for new buildings and other structures*. FEMA 750. Washington, DC: Building Seismic Safety Council, National Institute of Building.

Ghaboussi, J., and S. U. Dikmen. 1981. "Liquefaction analysis for multidirectional shaking." *J. Geotech. Eng.* 107 (5): 605–627. https://doi.org/10.1061/AJGEB6.0001133.

Green, R. A. 2001. "Energy-based evaluation and remediation of liquefiable soils." Ph.D. dissertation, Dept. of Civil and Environmental Engineering, Virginia Tech.

Groholski, D. R., Y. M. A. Hashash, B. Kim, M. Musgrove, J. Harmon, and J. P. Stewart. 2016. "Simplified model for small-strain nonlinearity and strength in 1D seismic response analysis." *J. Geotech. Geoenviron. Eng.* 142 (9): 04016042. https://doi.org/10.1061/(ASCE)GT.1943-5606.0001496.

Hashash, Y. M. A., M. I. Musgrove, J. A. Harmon, O. Ilhan, G. Xing, O. Numanoglu, D. R. Groholski, C. A. Phillips, and D. Park. 2020. *DEEPSOIL 7, user manual*. Urbana, IL: Univ. of Illinois at Urbana-Champaign.

Idriss, I. M., and R. W. Boulanger. 2010. *SPT-based liquefaction triggering procedures.* Rep. No. UCD/CGM-10, 2. Davis, CA: Univ. of California at Davis.

Ishihara, K., and Y. Koga. 1981. "Case studies of liquefaction in the 1964 Niigata earthquake." *Soils Found.* 21 (3): 35–52. https://doi.org/10.3208/sandf1972.21.3_35.

Jafarian, Y., I. Towhata, M. H. Baziar, A. Noorzad, and A. Bahmanpour. 2012. "Strain energy based evaluation of liquefaction and residual pore water pressure in sands using cyclic torsional shear experiments." *Soil Dyn. Earthquake Eng.* 35 (Sep): 13–28. https://doi.org/10.1016/j.soildyn.2011.11.006.

Jin, H., and L. Guo. 2021. "Effect of phase difference on the liquefaction behavior of sand in multidirectional simple shear tests." *J. Geotech. Geoenviron. Eng.* 147 (12): 06021015. https://doi.org/10.1061/(ASCE)GT.1943-5606.0002703.

Kayen, R. E., and J. K. Mitchell. 1997. "Assessment of liquefaction potential during earthquakes by Arias intensity." *J. Geotech. Geoenviron. Eng.* 123 (12): 1162–1174. https://doi.org/10.1061/(ASCE)1090-0241(1997)123:12(1162).

Kayen, R. E., R. E. S. Moss, E. M. Thompson, R. B. Seed, K. O. Cetin, A. Der Kiureghian, Y. Tanaka, and K. Tokimatsu. 2013. "Shear-wave velocity–based probabilistic and deterministic assessment of seismic soil liquefaction potential." *J. Geotech. Geoenviron. Eng.* 139 (3): 407–419. https://doi.org/10.1061/(ASCE)GT.1943-5606.0000743.

Kim, H. S., M. Kim, L. G. Baise, and B. Kim. 2021. "Local and regional evaluation of liquefaction potential index and liquefaction severity number for liquefaction-induced sand boils in Pohang, South Korea." *Soil Dyn. Earthquake Eng.* 141 (Aug): 106459. https://doi.org/10.1016/j.soildyn.2020.106459.

Ko, K. W., and R. E. Kayen. 2024. "Energy-based and strain-based methods for estimation of pore water pressure within liquefied soil layers." *J. Geotech. Geoenviron. Eng.* https://doi.org/10.1061/JGGEFK/GTENG-11458.

Kokusho, T. 2013. "Liquefaction potential evaluations: Energy-based method versus stress-based method." *Can. Geotech. J.* 50 (10): 1088–1099. https://doi.org/10.1139/cgj-2012-0456.

Kokusho, T. 2017. *Innovative earthquake soil dynamics*. 1st ed. London: Taylor & Francis.

Kokusho, T. 2021. "Energy–based liquefaction evaluation for induced strain and surface settlement—Evaluation steps and case studies." *Soil Dyn. Earthquake Eng.* 143 (Feb): 106552. https://doi.org/10.1016/j.soildyn.2020.106552.

Kokusho, T., and Y. Kaneko. 2018. "Energy evaluation for liquefaction-induced strain of loose sands by harmonic and irregular loading tests." *Soil Dyn. Earthquake Eng.* 114 (Jun): 362–377. https://doi.org/10.1016/j.soildyn.2018.07.012.

Kokusho, T., and S. Tanimoto. 2021. "Energy capacity versus liquefaction strength investigated by cyclic triaxial tests on intact soils." *J. Geotech. Geoenviron. Eng.* 147 (4): 04021006. https://doi.org/10.1061/(ASCE)GT.1943-5606.0002484.

Kostadinov, M. V., and F. Yamazaki. 2001. "Detection of soil liquefaction from strong motion records." *Earthquake Eng. Struct. Dyn.* 30 (2): 173–193. https://doi.org/10.1002/1096-9845(200102)30:2<173::AID-EQE3>3.0.CO;2-7.

Koyamada, K., Y. Miyamoto, and K. Tokimatsu. 2006. "Field investigation and analysis study of damaged pile foundation during the 2003 Tokachi-Oki earthquake." In *Proc., Seismic Performance and Simulation of Pile Foundations in Liquefied and Laterally Spreading Ground*, 97–108. Reston, VA: ASCE. https://doi.org/10.1061/40822(184)9.

Kramer, S. L., S. S. Sideras, and M. W. Greenfield. 2016. "The timing of liquefaction and its utility in liquefaction hazard evaluation." *Soil Dyn. Earthquake Eng.* 91 (Dec): 133–146. https://doi.org/10.1016/j.soildyn.2016.07.025.

Millen, M. D. L., A. Viana da Fonseca, and C. M. Azeredo. 2021. "Time–frequency filter for computation of surface acceleration for liquefiable sites: Equivalent linear Stockwell analysis method." *J. Geotech. Geoenviron. Eng.* 147 (8): 04021070. https://doi.org/10.1061/(ASCE)GT.1943-5606.0002581.

Moss, R. E., R. B. Seed, R. E. Kayen, J. P. Stewart, A. Der Kiureghian, and K. O. Cetin. 2006. "CPT-based probabilistic and deterministic assessment of in situ seismic soil liquefaction potential." *J. Geotech. Geoenviron. Eng.* 132 (8): 1032–1051. https://doi.org/10.1061/(ASCE)1090-0241(2006)132:8(1032).

Nemat-Nasser, S., and A. Shokooh. 1979. "A unified approach to densification and liquefaction of cohesionless sand in cyclic shearing." *Can. Geotech. J.* 16 (4): 659–678. https://doi.org/10.1139/t79-076.

Özener, P. T., M. W. Greenfield, S. S. Sideras, and S. L. Kramer. 2020. "Identification of time of liquefaction triggering." *Soil Dyn. Earthquake Eng.* 128 (Jan): 105895. https://doi.org/10.1016/j.soildyn.2019.105895.

Polito, C., R. A. Green, E. Dillon, and C. Sohn. 2013. "Effect of load shape on relationship between dissipated energy and residual excess pore pressure generation in cyclic triaxial tests." *Can. Geotech. J.* 50 (11): 1118–1128. https://doi.org/10.1139/cgj-2012-0379.

Polito, C. P. 2017. "Constant-volume cyclic testing to determine input parameters for the GMP pore pressure generation model." In *Geotechnical Frontiers 2017*, 71–79. Reston, VA: ASCE. https://doi.org/10.1061/9780784480489.008.

Polito, C. P., R. A. Green, and J. Lee. 2008. "Pore pressure generation models for sands and silty soils subjected to cyclic loading." *J. Geotech. Geoenviron. Eng.* 134 (10): 1490–1500. https://doi.org/10.1061/(ASCE)1090-0241(2008)134:10(1490).

Sasajima, T., A. Kubouchi, K. Miura, N. Otuka, and E. Kohama. 2004. "A project for the field observation of seismic behavior of full-sized test gravity type quay wall." In *Proc., 13th World Conf. on Earthquake Engineering*, 1–6. Vancouver, BC, Canada: WCEE Secretariat.

Sasajima, T., K. Miura, A. Kubouchi, N. Otsuka, E. Kohama, and J. Watanabe. 2005. "Liquefaction induced deformation of test quay wall in Kushiro Port during the 2003 Tokachi-Oki earthquake." In *Proc., Earthquake Engineering and Soil Dynamics*, 1–15. Reston, VA: ASCE. https://doi.org/10.1061/40779(158)15.

Seed, H. B., and I. M. Idriss. 1970. *Soil moduli and damping factors for dynamic response analyses*. Berkeley, CA: Univ. of California.

Seed, H. B., G. R. Martin, and R. M. Pyke. 1978. "Effect of multidirectional shaking on pore pressure development in sands." *J. Geotech. Eng.* 104 (1): 27–44. https://doi.org/10.1061/AJGEB6.0000575.

Seed, H. B., K. Tokimatsu, L. F. Harder, and R. M. Chung. 1985. "Influence of SPT procedures in soil liquefaction resistance evaluations." *J. Geotech. Eng.* 111 (12): 1425–1445. https://doi.org/10.1061/(ASCE)0733-9410(1985)111:12(1425).

Su, D., and X. S. Li. 2008. "Impact of multidirectional shaking on liquefaction potential of level sand deposits." *Géotechnique* 58 (4): 259–267. https://doi.org/10.1680/geot.2008.58.4.259.

Towhata, I., and K. Ishihara. 1985. "Shear work and pore water pressure in undrained shear." *Soils Found.* 25 (3): 73–84. https://doi.org/10.3208/sandf1972.25.3_73.

Unjoh, S., M. Kaneko, S. Kataoka, K. Nagaya, and K. Matsuoka. 2012. "Effect of earthquake ground motions on soil liquefaction." *Soils Found.* 52 (5): 830–841. https://doi.org/10.1016/j.sandf.2012.11.006.

Vucetic, M., and R. Dobry. 1986. *Pore pressure build-up and liquefaction at level sandy sites during earthquakes*. Research Rep. No. CE-86-3. Troy, NY: Rensselaer Polytechnic Institute.

Yamaguchi, A., T. Mori, M. Kazama, and N. Yoshida. 2012. "Liquefaction in Tohoku district during the 2011 off the Pacific coast of Tohoku earthquake." *Soils Found.* 52 (5): 811–829. https://doi.org/10.1016/j.sandf.2012.11.005.

Yamashita, S., Y. Ito, T. Hori, T. Suzuki, and Y. Murata. 2005. "Geotechnical properties of liquefied volcanic soil ground by 2003 Tokachi-Oki earthquake." In *Proc., 16th Int. Conf. on Soil Mechanics and Geotechnical Engineering*, 2737–2740. Amsterdam, Netherlands: IOS Press.

Youd, T. L., and I. M. Idriss. 2001. "Liquefaction resistance of soils: Summary report from the 1996 NCEER and 1998 NCEER/NSF workshops on evaluation of liquefaction resistance of soils." *J. Geotech. Geoenviron. Eng.* 127 (10): 297–313. https://doi.org/10.1061/(ASCE)1090-0241(2001)127:4(297).

Zeghal, M., et al. 2018. "Stress–strain response of the LEAP-2015 centrifuge tests and numerical predictions." *Soil Dyn. Earthquake Eng.* 113 (Oct): 804–818. https://doi.org/10.1016/j.soildyn.2017.10.014.

Zhang, J., T. Wang, S. Xiao, and L. Gao. 2021. "Chinese code methods for liquefaction potential assessment based on standard penetration test: An extension." *Soil Dyn. Earthquake Eng.* 144 (Feb): 106697. https://doi.org/10.1016/j.soildyn.2021.106697.